USF1 defect drives p53 degradation during Helicobacter pylori infection and accelerates gastric carcinogenesis

Lionel Costa, Sébastien Corre, Valérie Michel, Krysten Le Luel, Julien Fernandes, Jason Ziveri, Grégory Jouvion, Anne Danckaert, Nicolas Mouchet, David da Silva Barreira, et al.

USF1 defect drives p53 degradation during *Helicobacter pylori* infection and accelerates gastric carcinogenesis

Lionel Costa[1,2a], Sébastien Corre[3], Valérie Michel[1], Krysten Le Luel[1,2], Julien Fernandes[1,4], Jason Ziveri[1b], Grégory Jouvion[5c], Anne Danckaert[4], Nicolas Mouchet[3], David Da Silva Barreira[1d], Javier Torres[6], Margarita Camorlinga-Ponce[6], Mario Milco D'Elios[7], Laurence Fiette[5e], Hilde De Reuse[1], Marie-Dominique Galibert[3,8$] and Eliette Touati[1$*]

[1]*Helicobacter* Pathogenesis Unit, Institut Pasteur, CNRS ERL6002, Paris, (75015) France. [2]University Paris Diderot, Sorbonne Paris Cité, Paris, France. [3]Univ Rennes, CNRS, IGDR (Institut de Génétique et Développement de Rennes) – UMR6290, Rennes, (35000) France. [4]UtechS PBI – C2RT, Institut Pasteur, Paris, (75015) France. [5]Experimental Neuropathology Unit, Institut Pasteur, Paris, (75015) France. [6]Unidad de Investigacion en Enfermedades Infecciosas, UMAE Pediatria, IMSS, Mexico city, Mexico. [7]Department of Experimental and Clinical Medicine, University of Florence, Florence, Italy. Hospital University of Rennes (CHU Rennes), Department of Molecular Genetics and Genomics, Rennes, (35000) France.

Present address

[a]Institut Cochin, INSERM U1016, CNRS UMR 8104, Université Paris Descartes, Paris, (75014) France.
[b]INSERM U1151, CNRS UMR 8253, Institut Necker-Enfants Malades, Team 11: Pathogenesis of Systemic Infections, Paris, (75993) France.
[c]Sorbonne Université, INSERM, Pathophysiology of Pediatric Genetic Diseases, Assistance Publique-Hôpitaux de Paris, Hôpital Armand-Trousseau, UF Génétique Moléculaire, Paris, (75012) France
[d]University of Bourgogne, AgroSup, Laboratoire PAM UMR A 02.102, BP 27877, Dijon, (21000) France.
[e]IMMR, Institut Mutualiste Montsouris, 42 Boulevard Jourdan, Paris, (75014) France.

[$]Co-senior authors

Correspondence :
Eliette Touati, [1]*Helicobacter* Pathogenesis Unit, Institut Pasteur, CNRS ERL6002, Paris, (75015) France Phone: +33 1 40 61 37 85; Fax: +33 1 40 61 36 40
email: eliette.touati@pasteur.fr

Words count: 3949

ABSTRACT

Objective *Helicobacter pylori* (*Hp*) is a major risk factor for gastric cancer. *Hp* promotes DNA damage and proteasomal degradation of p53, the guardian of genome stability. *Hp* reduces the expression of the transcription factor USF1 shown to stabilize p53 in response to genotoxic stress. We investigated whether *Hp*-mediated USF1 deregulation impacts p53-response and consequently genetic instability. We also explored *in vivo* the role of USF1 in gastric carcinogenesis.

Design Human gastric epithelial cell lines were infected with *Hp*7.13, exposed or not to a DNA-damaging agent Camptothecin (CPT), to mimic a genetic instability context. We quantified the expression of *USF1*, *p53* and their target genes, we determined their sub-cellular localization by immunofluorescence and examined USF1/p53 interaction. *Usf1*$^{-/-}$ and INS-GAS mice were used to strengthen the findings *in vivo* and patient data examined for clinical relevance.

Results *In vivo* we revealed the dominant role of USF1 in protecting gastric cells against *Hp*-induced carcinogenesis and its impact on p53 levels. *In vitro*, *Hp* delocalizes USF1 into foci close to cell membranes. *Hp* prevents USF1/p53 nuclear built up and relocates these complexes in the cytoplasm, thereby impairing their transcriptional function. *Hp* also inhibits CPT-induced USF1/p53 nuclear complexes, exacerbating CPT-dependent DNA damaging effects.

Conclusion Our data reveal that the depletion of USF1 and its de-localization in the vicinity of cell membranes are essential events associated to the genotoxic activity of *Hp* infection, thus promoting gastric carcinogenesis. These findings are also of clinical relevance, supporting USF1 expression as a potential marker of gastric cancer susceptibility.

Key words: *Helicobacter pylori* Pathogenesis; Genetic Instability; DNA damage; Oncogenes, Gastric Cancer

Summary box

What is already known on this subject?

• *H. pylori* is a major risk factor for gastric cancer

• *H. pylori* promotes p53 proteasomal degradation and inhibits USF1 expression

• In response to DNA damaging agents, USF1 binds to p53 and inhibits its degradation

What are the new findings?

• Low USF1 and p53 levels are associated with low overall survival in human gastric cancer patients

• Loss of USF1 accelerates gastric carcinogenesis

• Only *H. pylori* and not genotoxic chemicals, leads to USF1 accumulation as structure-like foci at the periphery of the cells.

• *H. pylori* inhibits USF1/p53 nuclear interaction and impairs DNA repair function

How might it impact on clinical practice in the foreseeable future?

• **Depletion of USF1 in gastric tumoral tissue** can be an indicator of a poor prognosis and may become a new biomarker to identify sub-group of patients with higher risk of gastric cancer

• **Identification of drugs able to inhibit** cytoplasmic accumulation of USF1 or its nuclear depletion can allow future development of targeted therapies to improve gastric cancer treatment

INTRODUCTION

Helicobacter pylori (*Hp*) is responsible for about 90% of gastric cancer [GC] cases worldwide[1] [2,3], which represents the highest frequency of infectious agents-associated cancer (5.5%)[4]. Importantly, the detection of preneoplasia[5] and *Hp* eradication during early stages of the precancerous cascade can prevent GC development[6,7]. GC is an inflammation-driven disease resulting from the complex interplay between bacterial, host and environmental factors[8]. *Hp*-induced chronic inflammation contributes to neoplastic transformation, via dysregulation of signaling pathways, cell proliferation and genetic instability[9]. We previously reported that *Hp* induces mutations in chronically-infected mice[10,11,12]. *Hp* also causes DNA double strand breaks (DSB)[13,14] and impairs DNA repair pathways, favoring overall mutation load[12,15,16]. Importantly, *Hp* promotes the accumulation of mutations in the tumor suppressor gene *TP53*[17], which have been reported in 50% of gastric tumors[17,18]. In response to genotoxic stress, p53 activates signaling pathways leading to temporary cell cycle arrest allowing DNA damage and cellular repair[19]. Its inactivation promotes genome instability, a hallmark of cancer[20]. The inhibition of p53 has thus emerged as a strategy of bacterial pathogens to modulate host cellular functions[21], as for *Hp* which promotes p53 proteasomal degradation[22,23,24]. Together, this results in accumulation of oncogenic changes in infected cells.

Finally, *Hp* induces aberrant DNA methylation that down-deregulates the expression of genes related to signal transduction pathways and tumor suppression[25,26,27]. We reported that *Hp* induces DNA hypermethylation in the promoter region of the upstream stimulating transcription factors genes, *USF1* and *USF2*, inhibiting their expression in infected mice concomitantly to the development of gastric preneoplasia[28]. USF1 and USF2 are b-HLH-LZ transcription factors ubiquitously expressed. They regulate stress and immune responses, cell cycle control, inflammation and genome stability related genes[29]. They may thus act as tumor suppressors[30,31]. We previously showed that under ultra-violet (UV) stress, USF1 up-regulates

CSA and *HR23A* genes expression, two actors of the transcription-coupled and global genome nucleotide excision repair pathway (TC-NER and GG-NER), respectively[32]. USF1 also binds p53 in response to UV-induced DNA damage, preventing the E3-ubiquitin ligase HDM2-p53 interaction. This results in p53 stabilization and transient cell cycle arrest[33]. How USF1 modulates p53 levels in response to *Hp* and the consequences on the infection-associated genotoxicity have never been addressed.

In the present study, we investigate the role of both USF1 and p53 transcription factors in gastric carcinogenesis and asked whether USF1 deregulation during *Hp* infection could impact the p53-response and increase genetic instabilities. Using a mouse model, we showed that the absence of USF1 has strong implications in the oncogenic properties of *Hp*, triggering the severity of gastric lesions. In line with these data, low expression levels of both *USF1* and *TP53* and consequently deregulation of their target genes, are observed in a significant number of GC patients, associated with a worse prognosis. Our findings show that USF1 is a key player in the complex regulatory network linking *Hp* infection to gastric carcinogenesis and pave the way to a better understanding of the mechanisms at the origin of pathogen-induced cancer.

RESULTS

Low USF1 and p53 levels are associated with a worse prognosis in GC patients

Using The Cancer Genome Atlas (TCGA) data sets, GC patients [STAD] are distinguished according to their overall survival (top 25% low *versus* top 25% high, n=188), based on *SLC7A2* expression, the most discriminant gene (figure S1A). As observed in the expression heatmap (figure 1A), *USF1* and *TP53* gene expression levels are correlated with the GC patients overall survival. Low mRNA levels of both *USF1* and *TP53* are associated with poor 3-year survival (figures 1B and S1B). Moreover, for every patient, the mRNA expression levels of USF1 and p53 are correlated (figure S1C) and consequently impact their transcriptional function leading to a significant down-regulation of pathways, notably p53-signaling, DNA repair (BER, NER)

and cell cycle regulation, in patients with low *vs* high survival (figure S1D). In order to identify the p53 and USF1-target genes significantly enriched in the two groups (low *vs* high survival), we performed Gene Set Enrichment Analysis (http://software.broadinstitute.org/cancer/software/gsea) in GC, TCGA dataset [STAD] (figure S1E-F). The median expression of the top-genes enriched in the low and high survival groups (figure S2), showed a specific survival rate-dependent expression on both USF1- and p53-target genes (figure 1C). Interestingly, the analysis of another data set from Hippo and coll[34] (GSE2685), confirmed the decrease of most of USF1 and p53-regulated genes expression in GC patients, in tumoral *vs* normal tissues (figure 1D). In parallel, we analyzed *USF1* gene expression in gastric biopsies from GC patients. In 50% of these patients, *USF1* expression was lower in the tumoral *vs* adjacent non-tumoral tissue (fold-change <1; 17/34 patients; P<0.0001) (figure 1E), and 88% (15/17) of patients with low *USF1* expression were *Hp*-positive (figure S1G). These data suggest that *Hp*-associated decrease of *USF1* gene expression may define a sub-group of more aggressive gastric tumors. The consequences of *Hp* infection on both USF1 and p53 target-genes expression were also analysed in gastric cells using expression data from Koeppel and coll[16] (GSE55699) and Hong and coll (E-GEOD-74577). A significant decrease of *USF1* and *TP53* mRNA levels and target genes, mainly correlated with low survival was observed (figure 1F). These features are also confirmed in *Hp*-infected mice using both expression data from Galamb and coll[35] (GSE5081) (figure S3A) and our previous study[36] (E-MEXP-1135) (figure S3B).

The absence of USF1 exacerbates the severity of* Hp-*induced gastric lesions

To determine the consequences of the absence of USF1 in *Hp*-associated gastric pathogenesis, we infected *Usf1*-KO mice (*Usf1*$^{-/-}$)[37] and the parental mice (*Usf1*$^{+/+}$) with *Hp*SS1 strain which colonizes the mouse stomach[38]. At each time-point (9/12 months), the infection

status was monitored (figure S3C) and histological analysis performed (figure 2A-B). Nine-months post-infection (pi), both *Usf1*$^{-/-}$ and *Usf1*$^{+/+}$ mice developed gastric lesions, consisting in infiltration of inflammatory cells, mainly mononucleated cells, in the mucosa and sub-mucosa (figure 2A). A semi-quantitative analysis showed an exacerbation of metaplasia and dysplasia in *Usf1*$^{-/-}$ mice compared to *Usf1*$^{+/+}$ (figure 2B). After 9 months, only *Hp*-infected *Usf1*$^{-/-}$ mice showed metaplasia and dysplasia that were absent in *Usf1*$^{+/+}$ infected mice. An important loss of parietal cells favoring hypochlorhydria and atypia was also observed in *Usf1*$^{-/-}$ infected mice. In *Hp*-infected *Usf1*$^{+/+}$ mice, these atypia and dysplasia appeared only after 12 months. At 12 months pi, the gastric inflammation was significantly more severe in *Hp*-infected *Usf1*$^{-/-}$ mice, with score-grading of 2.5 for intestinal metaplasia and parietal cell loss, compared to 1 in *Usf1*$^{+/+}$ mice. In addition, immunofluorescence (IF) analysis of gastric tissue sections shows that in the absence of USF1 (*Usf1*$^{-/-}$ mice), *Hp* infection strongly promotes p53 loss (figure 2C). This leads to a down regulation of its target genes (*GADD45, CDKN1A, PCNA, RAB31*) (Figure S3D), in agreement with previous mice data[35,36] (figure S3A-B). Together, these results underscored for the first time a role for USF1 in gastric carcinogenesis.

Hp *impairs DNA repair functions by downregulating USF1 and p53*

Since USF1 and p53 cooperate to maintain genetic stability, we investigated whether *Hp* impacts USF1/p53 functioning. We first showed that at 2 and 24h after infection of MKN45 gastric epithelial cells, the expression of *USF1* and *TP53* genes was significantly diminished by the oncogenic strain *Hp*7.13[39] (figure 3A, C, E), with a significant and concomitant decrease of their protein levels at 24h pi (figure 3B, 3D). This resulted in the diminution of the expression of USF1 and p53 DNA repair target genes: respectively *CSA*, *HR23A* and *GADD45A* (figure 3F). Similar results were obtained with cells treated with *Hp*7.13 total extracts (50 and 100 µg/ml), (figure S4A-E), concomitantly with an increase in DNA damage hallmark

(phosphorylated-histone H2AX, γH2AX) (figure S4F). The infection of MKN45 cells with *Hp*SS1 also, inhibited USF1 and p53 levels (figure S5). These data, suggest that *Hp*-mediated decrease of USF1 and p53 impacts the DNA repair ability of infected cells and consequently affect their genetic stability.

Hp *leads to USF1 foci accumulation in the cytoplasm and membrane-surrounding regions of gastric cells*

Hp has previously been reported to promote the cytoplasmic p53 proteasomal degradation[22,23]. USF1 was shown to interact with p53 leading to p53 nuclear stabilization in response to genotoxic stress[33]. Using immunofluorescence (IF), we observed that, at 2h pi, p53 nuclear staining was significantly lower in *Hp*-infected cells than in non-infected, as also USF1 nuclear staining (figure 4A-B). More importantly, we detected cytoplasmic USF1 foci-like structures, mainly in the membrane-surrounding area of *Hp*-infected cells at 2 and 24h (figure 4A and C; yellow arrows). Quantification of these foci revealed a marked increase with infection time (figure 4C), being present in 80% of *Hp*-infected cells at 24h pi. Importantly, a cytoplasmic accumulation of USF1 was also observed in *Hp*-infected INS-GAS mice after 6/12 months in the presence of gastric intraepithelial neoplasia (figure S6A-B), with a p53 decrease as reported at 12 months pi (figure S6C). Together these results indicate that *Hp* relocates USF1 outside of the nucleus, and promotes USF1 cytoplasmic/membrane accumulation, concomitantly to p53 degradation.

To strengthen this point, we used the well-known DNA-damaging compound, camptothecin (CPT), amplifying the USF1 and p53 genotoxic stress response, as previously reported[33]. Briefly, cells were exposed to CPT (50nM) and infected by *Hp* or not for 2 and 24h. As anticipated, CPT alone induced an immediate DNA-damage response, showed by γH2AX staining (figure S7), promoting a strong p53 nuclear accumulation 24h post CPT-treatment

(figure 5A). This p53 increase was significantly reduced in infected cells, as shown by IF quantification (figure 5B). In parallel, while the impact on USF1 expression was mild (figure 5A-B), an important cytoplasmic/membrane accumulation of USF1 foci was observed in CPT-treated cells only in the presence of *Hp*, as confirmed by spots quantification (figure 5A, C). Comparable results were obtained when *Hp*-infection was combined with different genotoxic stress compounds (MMS, H_2O_2) (figures S8-S9). Together this strongly supports the important and specific role of *Hp* on USF1 and p53 biological function.

Hp *impairs the formation of USF1/p53 complexes*

To investigate the mechanism by which *Hp* impairs USF1 and p53 function, we followed the formation of USF1/p53 complexes in response to CPT-induced genotoxic stress and infection using proximity ligation assay (PLA)[40]. According to its genotoxic activity, CPT alone induces nuclear USF1/p53 complexes, with a marked increase after 24h. In CPT-treated/*Hp*-infected cells, the formation of these complexes is abrogated. Thus, CPT exacerbated *Hp*-mediated effects with a stronger inhibition of the formation of USF1/p53 complexes, compared to *Hp* infection alone (figure 6A-B). Together, this shows that minute nuclear amounts of USF1 in infected cells are associated with the absence of USF1/p53 nuclear complexes, impairing p53 stabilization in agreement with its *Hp*-mediated degradation[22,23].

Hp *infection sensitizes gastric cells to genotoxic stress*

We next investigated whether *Hp* infection could sensitize cells to DNA-damage. To address this important clinical question, cells were first infected with *Hp*7.13 for 24h, washed several times prior to their treatment with CPT (50nM) for 24h (figure 7A). Here also, *Hp*-infected cells displayed accumulation of USF1 foci mainly at their periphery with low p53 staining, while CPT-treatment alone, promotes USF1 and p53 nuclear increase (figure 7B). Sensitizing

cells with *Hp* 24h prior to CPT-treatment still leads to an important accumulation of USF1 foci in the cytoplasm and surrounding-membrane cell area (figure 7B). Importantly, we noticed the presence of p53-positive micronuclei-like structures (figure 7B, yellow arrows), a signature of elevated genotoxic stress[41] known to accumulate p53[42], as under our conditions. Same results were observed with MMS and H_2O_2-treated cells (1mM) (figure S10). Thus, *Hp*-induced USF1 cytoplasmic/peripheral accumulation is maintained post-infection, rendering the cells more susceptible to DNA-damaging agents.

DISCUSSION

The impairment of p53 function plays a key role in the promotion of carcinogenesis. We previously showed that UV-induced p53 stabilization and subsequent transient cell-cycle arrest requires USF1[33]. Up to now, no direct *in vivo* evidence linking USF1 to cancer was provided, although molecular data were in favor of such a role[30,43, 44]. Studies associated *USF1* polymorphisms with increased risk of cancer[45,46,47]. Here we demonstrate for the first time that loss of USF1 promotes *Hp*-induced carcinogenesis. First, the *in vivo* absence of USF1 in *Usf1*$^{-/-}$ mice, leads to p53 depletion and accelerates the development and triggers the severity of *Hp*-induced gastric lesions. More importantly, these mice recapitulate the sequential gastric pre-neoplastic cascade described in human pathology[3]. *Usf1*$^{-/-}$ mice constitute thus an interesting model to study *Hp*-induced gastric carcinogenesis. Second, in human GC samples, *USF1* and *TP53* gene expression is associated with patient prognosis (TCGA analysis), as low transcriptional levels correlate with poor 3-years survival. Moreover, *USF1* and *TP53* expression levels directly impact their target genes such as those related to DNA repair, cell cycle regulation and p53 signaling pathways. Furthermore, low *USF1* gene expression in GC patients is mainly associated with *Hp* status. Thus, *Hp*-positive gastric tumors with low *USF1 and TP53* levels may identify a subgroup of patients with poor prognosis. Together these data

demonstrate that USF1 has tumor suppressive functions and that its low level should be considered as a potential marker of cancer susceptibility.

We also show that *Hp* infection delocalizes the nuclear factor USF1 at the periphery of cells into foci that resemble aggregates. This occurs concomitantly with a diminution of its nuclear amount, as schematized in figure 8A. This phenotype is only observed in *Hp*-infected cells and not after exposure to DNA damaging agents. The unexpected cellular localization of USF1 may impair its transcriptional regulatory function, reducing the expression of its NER target genes *CSA* and *HR23A* in infected cells. It also controls its biological function, impairing nuclear USF1/p53 complex formation. Indeed, *Hp*-mediated USF1 depletion diminishes the stabilization of p53 that is known to contribute to genetic instability and oncogenic properties of the infection.

USF1 as part of the b-HLH-LZ transcription factor family is well known for its nuclear function[29]. The *Hp*-mediated delocalization of USF1 outside the nucleus was unexpected. The underlying mechanism and the cellular structure involved remain to be clarified. It may well be that *Hp*-infection induces USF1 post-translational modifications modulating its nuclear-cytoplasmic trafficking, that results in its cytoplasmic/membrane accumulation. This could represent an *Hp* strategy to prevent USF1 transcriptional function, impairing its tumor suppressive activity and DNA repair functions. Alternatively, USF1 foci could correspond to protein aggregation due to infection-induced misfolding, as recently reported the formation of aggresomes by Twist1, another b-HLH-LZ transcription factor [48].

In response to a genotoxic stress, USF1 and p53 interact promoting p53 stabilization and blocking its interaction with the E3-ubiquitin ligase HDM2, thereby abrogating subsequent p53 degradation[33]. We show that nuclear depletion of USF1 parallels the p53 decrease in *Hp*-infected cells. Under this condition, we speculate that the nuclear level of USF1 is too low to ensure p53 stabilization, limiting the formation of USF1/p53 complexes. Importantly, infection

of cells by *Hp* prior to CPT- (MMS or H_2O_2) treatment maintains the cytoplasmic/membrane delocalization of USF1, indicating that once initiated this process is sustained even in the absence of a new *Hp* challenge. *Hp*-induced accumulation of USF1 outside the nucleus could thus constitute a "point of no return", after which USF1 is no more available to undertake its nuclear functions. This suggests that *Hp*-infection may weaken DNA repair ability of cells exposed to genotoxic stress. As illustrated in figure 8B, *Hp* can persist all lifelong, promoting DNA damage, which thus results from the combined effects of the infection and exposure to genotoxic environmental factors, increasing the risk of GC.

In conclusion, this study demonstrated that USF1 is a new central regulator of DNA damage and repair in response to *Hp* infection. The absence of USF1 results in the promotion of gastric carcinogenesis as demonstrated *in vivo* with the *Usf1*$^{-/-}$ mice, which constitute a new powerful tool to deepen our understanding of the molecular cascade from pre-neoplasia to GC development. Our findings are also of clinical relevance and pave the way to propose the USF1 level as a potential biomarker for GC.

METHODS

Cells culture and bacteria growth conditions, mice infection and histology, analysis of genes expression, proteins and imaging procedures and data banks used in *in silico* study are reported in the supplementary information.

Bacteria and cells

Human gastric epithelial cells, MKN45 (received from C. Reis's laboratory, Porto, Portugal), were used in this study and infected with *Hp* strains 7.13[39] and SS1[38].

Analysis of protein complexes by proximity ligation assay (PLA)

The USF1/p53 complexes were visualized by Duolink proximity ligation assay (PLA)[40], as reported in the supplementary information. Imaging analysis was carried out using an inverted widefield microscope Axio Observer Z1 equipped with Apotome grid (Carl Zeiss, Germany).

Human gastric biopsies

All patients were adults, informed and signed a consent letter. The study was approved by the Local Ethical Committees from the National Council for Research on Health, IMSS, Mexico and Florence University Hospital, Italy.

Gastric biopsies (tumoral and adjacent tissue) were from GC patients who attended the Instituto Mexicano del Seguro Social (IMSS), Medical Center SXXI in Mexico (n=28) and the Florence University Hospital (n=6). For each patient, diagnosis was based on endoscopic examination and histopathologic analysis.

Hp *infection in mice*

Mice experiments were carried out according to the European Directives (2010/63/UE). The project was approved by the Comité d'Ethique en Expérimentation Animale (CETEA), Institut Pasteur (Ref 00317.02) and the Federative Structure of Research, Rennes (Ref APAFIS#905-2015060515515795 v4).

Usf1$^{-/-}$[37] and *Usf1*$^{+/+}$ mice (C57BL/6j 129SV) were from S. Vaulont (Institut Cochin, Paris, France) and INS-GAS mice[49,50] from TC Wang (Columbia University College, NY, USA).

Statistical Analysis

Statistical analysis was performed using the Student-t test or Mann-Whitney test, after being assessed for normality of samples distribution. Results were considered significant if $p<0.05$. Kaplan-Meier survival analysis assumption was performed on the TCGA data set (https://cancergenome.nih.gov).

Acknowledgments We thank Sophie Vaulont (Institut Cochin, Paris, France) for Usf1$^{-/-}$ mice, Timothy C Wang (Columbia University, NY, USA) for providing us couples of INS-GAS mice and Joana Gomes and Celso Reis (I3S-IPATIMUP, Porto, Portugal) for MKN45 cells. We also thank Laurence Bernard-Touami and the Animal Housing ARCHE (UMS Biosit, https://biosit.univ-rennes1.fr, University of Rennes, France), and David Hardy and Magalie Tichit (Unit of Experimental Neuropathology, Institut Pasteur, Paris, France) for her technical help on the histology part and the UtechS Photonic BioImaging (Imagopole), C2RT, Institut Pasteur, supported by the French National Research Agency (France BioImaging; ANR-10–INSB–04; Investments for the Future), both as a part of the FranceBioImaging infrastructure.

Contributors Study concept and design: LC, SC, MDG, ET; experiments and acquisition of data: LC, SC, VM, KLL, JF, JZ, GJ, NM, DDSB, LF, ET; analysis of data and statistics: LC, SC, AD, MDG, ET; patient data and samples collection: JT, MCP, MMD; drafting of the manuscript: SC, MDG, ET; critical revision of the manuscript: JT, MMD, HDR; reading and approval of the manuscript: all authors; study supervision and funding: MDG, ET

Funding This work was supported by funding from the Odyssey Reinsurance Company to ET, the West committee of the Ligue Nationale Contre le Cancer (LNCC) and the UMS Biosit to MDG. JT received financial support from Fondo de Investigacion en Salud, IMSS, Mexico (FIS/IMSS/PROT/PRIO/13/027). The LNCC provided a doctoral fellowship to LC and the Odyssey Reinsurance company financed JF postdoctoral fellowship. KLL is a doctoral fellow from the University Paris Diderot, Ecole Doctorale Bio Sorbonne Paris Cité (BioSPC).

Competing interests None declared

References

1. Peek RMJ, Blaser MJ. *Helicobacter pylori* and gastrointestinal tract adenocarcinomas. *Nat Rev Cancer* 2002;2:28-37.
2. Kim SS, Ruiz VE, Carroll JD, *et al. Helicobacter pylori* in the pathogenesis of gastric cancer and gastric lymphoma. *Cancer Lett* 2011;305:228-38.
3. Correa P. Human gastric carcinogenesis : a multistep and multifactorial process. First American Cancer Society Award Lecture on Cancer Epidemiology and Prevention. *Cancer Res* 1992;52:6735-40.
4. Plummer M, de Martel C, Vignat J, *et al.* Global burden of cancers attributable to infections in 2012: a synthetic analysis. *The Lancet Global health* 2016;4:e609-16.
5. Pimentel-Nunes P, Libanio D, Marcos-Pinto R, *et al.* Management of epithelial precancerous conditions and lesions in the stomach (MAPS II): European Society of Gastrointestinal Endoscopy (ESGE), European Helicobacter and Microbiota Study Group (EHMSG), European Society of Pathology (ESP), and Sociedade Portuguesa de Endoscopia Digestiva (SPED) guideline update 2019. *Endoscopy* 2019;51:365-88.
6. Malfertheiner P, Mégraud F, O'Morain CA, et al. Management of *Helicobacter pylori* infection-the Maastricht V/Florence Consensus Report. *Gut* 2017;66:6-30.
7. Rugge M, Genta RM, Di Mario F, et al. Gastric Cancer as Preventable Disease. *Clin Gastroenterol Hepatol: the official clinical practice journal of the American Gastroenterological Association* 2017;15:1833-43.
8. Mommersteeg MC, Yu J, Peppelenbosch MP, *et al.* Genetic host factors in *Helicobacter pylori*-induced carcinogenesis: Emerging new paradigms. *Bioch Biophys Acta Rev Cancer* 2018;1869:42-52.
9. Hardbower DM, de Sablet T, Chaturvedi R, *et al.* Chronic inflammation and oxidative stress: the smoking gun for *Helicobacter pylori*-induced gastric cancer? *Gut Microbes* 2013;4:475-81.
10. Touati E, Michel V, Thiberge J, *et al*. Chronic *Helicobacter pylori* infections induce gastric mutations in mice. *Gastroenterology* 2003;124:1408-19.
11. Touati E, Michel V, Thiberge JM, *et al.* Deficiency in OGG1 protects against inflammation and mutagenic effects associated with *H. pylori* infection in mouse. *Helicobacter* 2006;11:494-505.
12. Machado A, Figuereido C, Touati E, *et al. Helicobacter pylori* infection downregulates nuclear and mitochondrial DNA repair in gastric cells. *Clin Can Res* 2009;15:2995-3002.

13. Toller IM, Neelsen KJ, Steger M, *et al.* Carcinogenic bacterial pathogen Helicobacter pylori triggers DNA double-strand breaks and a DNA damage response in its host cells. *Proc Natl Acad Sci U S A* 2011;108:14944-9.
14. Hartung ML, Gruber DC, Koch KN, *et al. H. pylori*-induced DNA strand breaks are introduced by nucleotide excision repair endonucleases and promote NF-kappaB target gene expression. *Cell Rep* 2015;13:70-9.
15. Kim JJ, Tao H, Carloni E, *et al. Helicobacter pylori* impairs DNA mismatch repair in gastric epithelial cells. *Gastroenterology* 2002;123:542-53.
16. Koeppel M, Garcia-Alcalde F, Glowinski F, *et al. Helicobacter pylori* infection causes characteristic DNA damage patterns in human cells. *Cell Rep* 2015;11:1703-13.
17. Matsumoto Y, Marusawa H, Kinoshita K, *et al. Helicobacter pylori* infection triggers aberrant expression of activation-induced cytidine deaminase in gastric epithelium. *Nat Med* 2007;13:470-6.
18. Wada Y, Takemura K, Tummala P, *et al. Helicobacter pylori* induces somatic mutations in TP53 via overexpression of CHAC1 in infected gastric epithelial cells. *FEBS Open bio* 2018;8:671-79.
19. Meek DW. Tumour suppression by p53: a role for the DNA damage response? *Nat Rev Cancer* 2009;9:714-23.
20. Eischen CM. Genome Stability Requires p53. *Cold Spring Harb Perspect Med* 2016;6
21. Chumduri C, Gurumurthy RK, Zietlow R, *et al.* Subversion of host genome integrity by bacterial pathogens. *Nat Rev Mol Cell Biol* 2016;17:659-73.
22. Wei J, Nagy TA, Vilgelm A, *et al.* Regulation of p53 tumor suppressor by *Helicobacter pylori* in gastric epithelial cells. *Gastroenterology* 2010;139:1333-43.
23. Buti L, Spooner E, Van der Veen AG, *et al. Helicobacter pylori* cytotoxin-associated gene A (CagA) subverts the apoptosis-stimulating protein of p53 (ASPP2) tumor suppressor pathway of the host. *Proc Natl Acad Sci U S A* 2011;108:9238-43.
24. Coombs N, Sompallae R, Olbermann P, *et al. Helicobacter pylori* affects the cellular deubiquitinase USP7 and ubiquitin-regulated components TRAF6 and the tumour suppressor p53. *Int J Med Microb* 2011;301:213-24.
25. Maekita T, Nakazawa K, Mihara M, *et al.* High levels of aberrant DNA methylation in *Helicobacter pylori*-infected gastric mucosae and its possible association with gastric cancer risk. *Clin Can Res* 2006;12:989-95.
26. Touati E. When bacteria become mutagenic and carcinogenic: lessons from *H. pylori*. *Mutat Res* 2010;703:66-70.

27. Servetas SL, Bridge DR, Merrell DS. Molecular mechanisms of gastric cancer initiation and progression by *Helicobacter pylori. Curr Op Infect Dis* 2016;29:304-10.

28. Bussière FI, Michel V, Memet S, *et al. H. pylori*-induced promoter hypermethylation downregulates USF1 and USF2 transcription factor gene expression. *Cell Microbiol* 2010;12:1124-33

29. Corre S, Galibert MD. Upstream stimulating factors: highly versatile stress-responsive transcription factors. *Pig Cell Res* 2005;18:337-48.

30. Ismail P, Lu T, Sawadogo M. Loss of USF transcriptional activity in breast cancer cell lines. *Oncogene* 1999;18:5582-91.

31. Chen N, Szentirmay MN, Pawar SA, *et al.* Tumor-suppression function of transcription factor Usf2 in prostate carcinogenesis. *Oncogene* 2006;25:579-87.

32. Baron Y, Corre S, Mouchet N, *et al.* USF-1 is critical for maintaining genome integrity in response to UV-induced DNA photolesions. *PLoS Genet* 2012;8:e1002470.

33. Bouafia A, Corre S, Gilot D, *et al.* p53 requires the stress sensor USF1 to direct appropriate cell fate decision. *PLoS Genet* 2014;10:e1004309.

34. Hippo Y, Taniguchi H, Tsutsumi S, *et al.* Global gene expression analysis of gastric cancer by oligonucleotide microarrays. *Cancer Res* 2002;62:233-40.

35. Galamb O, Gyorffy B, Sipos F, *et al. Helicobacter pylori* and antrum erosion-specific gene expression patterns: the discriminative role of CXCL13 and VCAM1 transcripts. *Helicobacter* 2008;13:112-26.

36. Vivas JR, Regnault B, Michel V, *et al.* Interferon gamma-signature transcript profiling and IL-23 upregulation in response to *Helicobacter pylori i*nfection. *Int J Immun Pharm* 2008;21:515-26.

37. Vallet VS, Casado M, Henrion AA, *et al.* Differential roles of upstream stimulatory factors 1 and 2 in the transcriptional response of liver genes to glucose. *J Biol Chem* 1998;273:20175-9.

38. Lee A, O'Rourke J, Ungria M, *et al.* A standardized mouse model of *Helicobacter pylori* infection : introducing the Sydney strain. *Gastroenterology* 1997;112:1386-97.

39. Franco AT, Israel DA, Washington MK, et al. Activation of beta-catenin by carcinogenic *Helicobacter pylori. Proc Natl Acad Sci U S A* 2005;102:10646-51.

40. Soderberg O, Gullberg M, Jarvius M, *et al.* Direct observation of individual endogenous protein complexes in situ by proximity ligation. *Nat Met* 2006;3:995-1000.

41. Luzhna L, Kathiria P, Kovalchuk O. Micronuclei in genotoxicity assessment: from genetics to epigenetics and beyond. *Front Genet* 2013;4:131.

42. Granetto C, Ottaggio L, Abbondandolo A, *et al*. p53 accumulates in micronuclei after treatment with a DNA breaking chemical, methylnitrosourea, and with the spindle poison, vinblastine. *Mutat Res* 1996;352:61-4.

43. Horbach T, Gotz C, Kietzmann T, *et al.* Protein kinases as switches for the function of upstream stimulatory factors: implications for tissue injury and cancer. *Front Pharm* 2015;6:3.

44. Chang JT, Yang HT, Wang TC, *et al.* Upstream stimulatory factor (USF) as a transcriptional suppressor of human telomerase reverse transcriptase (hTERT) in oral cancer cells. *Mol Carc* 2005;44:183-92.

45. Zhao X, Wang T, Liu B, *et al.* Significant association between upstream transcription factor 1 rs2516839 polymorphism and hepatocellular carcinoma risk: a case-control study. *Tumour Biol : J Intern Soc Oncodev Biol Med* 2015;36:2551-8.

46. Zhou X, Zhu HQ, Ma CQ, *et al.* Two polymorphisms of USF1 gene (-202G>A and -844C>T) may be associated with hepatocellular carcinoma susceptibility based on a case-control study in Chinese Han population. *Med Oncol* 2014;31:301.

47. Yuan Q, Bu Q, Li G, *et al.* Association between single nucleotide polymorphisms of upstream transcription factor 1 (USF1) and susceptibility to papillary thyroid cancer. *Clin Endocrin* 2016;84:564-70.

48. Govindarajalu G, Selvam M, Palchamy E, *et al.* N-terminal truncations of human bHLH transcription factor Twist1 leads to the formation of aggresomes. *Mol Cell Biochem* 2018;439:75-85.

49. Fox J, Rogers A, Ihrig M, *et al. Helicobacter pylori* associated gastric cancer in INS-GAS mice is gender specific. *Can Res* 2003;63:942-50.

50. Wang T, Dangler C, Chen D, *et al.* Synergistic interaction between hypergastrinemia and Helicobacter infection in a mouse model of gastric cancer. *Gastroenterology* 2000;118:36-47.

Legend of figures

Figure 1. Correlation of p53 and USF1 loss with gastric carcinogenesis and *Hp* infection. (A) Expression Heatmap depicting mRNA expression of genes distinguishing most significantly GC patients according to their overall survival. Expression data for (low survival: 665 days or high survival: 1095 days) were obtained from TCGA (STAD, n=188) (see Supplementary figure S1A). (B) Survival curve for GC patients according to *USF1* and *TP53* mRNA levels (low: green, medium: blue or high: red). (C) Expression Heatmap depicting median mRNA expression of p53 target genes (Fisher_direct_p53_targets_meta_analysis, GSEA) and putative USF1 target genes (Genes having at least one occurrence of transcription factor binding site V$USF_01 (v7.4 TRANSFAC) in the regions spanning up to 4 kb around their transcription starting sites, GSEA, significantly enriched in both low and high survival GC patients (top 50 genes, see supplementary figure S1E-F). (D) Expression Heatmap depicting p53 and USF1-target genes expression (p53-targets: orange and pink; USF1-targets: blue and green; common: black), previously correlated with low (pink and green) or high survival (orange and blue) using data from Hippo and coll[34] comparing noncancerous and cancerous tissues. (E) Relative *USF1* gene expression in gastric biopsies from GC patients (n=34) measured by qRT-PCR (tumoral *vs* adjacent tissue); bar: median value. Mann-Whitney test (low (<1) vs high (>1) expression; ****p<0.0001). (G) Log-fold enrichment of p53- and USF1-target genes expression in *Hp*-infected gastric cells. Data from GSE55699 (Koeppel and coll)[16] and E-GEOD-74577 (Hong and coll.).

Figure 2. Loss of USF1 exacerbates gastric tumorigenesis associated to *Hp* infection. *Usf1*$^{-/-}$ and *Usf1*$^{+/+}$ mice were oro-gastrically infected with *Hp*SS1 for 9 and 12 months as described in the supplementary methods (A) Representative gastric histological changes on H&E stained tissue section, in *Usf1*$^{-/-}$ (d, e, f, j, k ,l) and *Usf1*$^{+/+}$ (a, b, c, g, h, i) mice, *Hp*-

infected (b, c, e, f, h, i, j, k,l) and non-infected (a, d, g, j), after 9 months (a-f) and 12 months (g-l). As early as 9 months, cysts and atypia are observed in *Usf1*$^{-/-}$-infected mice (arrows). Dysplasia is only detected in *Usf1*$^{-/-}$ infected mice at 9 months pi (arrows). (B) Semi-quantitative evaluation of gastric lesions in *Hp*-infected *Usf1*$^{-/-}$ and *Usf1*$^{+/+}$ mice (see supplementary information). Mann-Whitney test, infected *vs* non-infected (*, $p<0.05$). (C) p53 IF (green) and nuclei (Hoechst, blue) on gastric tissue sections from *Hp*-infected *Usf1*$^{-/-}$ and *Usf1*$^{+/+}$ mice at 12 months pi, showing a depletion of p53 in *Hp*-infected *Usf1*$^{-/-}$ mice. Scale bar 100µm.

Figure 3. *Hp* impairs host DNA repair function by down-regulating USF1 and p53.

MKN45 cells were infected with *Hp*7.13 (MOI 100:1) for 2 and 24h. Control cells were not infected. (A) *USF1* (C) *TP53* (E) paired *USF1-TP53* (F) *CSA, HR23A* and *GADD45A* mRNA level quantified by RT-qPCR. Results are relative to the *18SrRNA*. Mean±SD, n=3. (B) WB analysis of (B) USF1 (E) p53 and GAPDH (loading control) in protein extracts from infected and non-infected cells. The histogram below corresponds to immunoblot quantification. Error bars: SD, n=3. Student t test, infected *vs* non-infected (*$p<0.05$; **$p<0.01$; ****$p<0.0001$).

Figure 4. *Hp* leads to USF1 foci in the vicinity of cell membranes.

(A) Immunofluorescence analysis of USF1 and p53 levels and localization in MKN45 cells infected as in figure 3. p53 immunostaining (red), USF1 (green) and nuclei (Hoechst, blue). Phalloidin actin staining (grey) indicates the cells shape. Scale bar 5µm. (B) Quantification of USF1 and p53 nuclear IF intensity (n=150-220 cells/condition). Mann-Whitney test, infected *vs* non-infected (*$p<0.05$; ****$p<0.0001$). (C) Maximum intensity projection of representative *Hp*-infected and non-infected cells at 24h. USF1 staining (green) shows foci (yellow arrows) in the cytoplasm and vicinity of cell membranes in infected-cells (left part). Quantification of

USF1 spots number per cell according to defined spot criteria as indicated in material and methods (right panel) (n=150-220 cells/condition). Experiments in triplicate with 5-7 microscopic fields analysed. Mann-Whitney test, infected *vs* non-infected (*p<0.05; ****p<0.0001).

Figure 5. USF1 foci are specifically induced by *Hp* infection.

(A) IF analysis of USF1 and p53 levels and localization, in MKN45 cells treated or not with CPT(50nm) and infected with *Hp* 7.13 for 2 and 24h. p53 (red), USF1 (green), nuclei (Hoechst, blue) and phalloidin actin staining (grey). The delocalization and accumulation of USF1 are specifically observed in the cytoplasm and membrane surrounding area of *Hp*-infected/CPT-treated cells. Scale bar 5µm. (B) Quantification of USF1 and p53 nuclear IF intensity (n=150-220 cells/condition). (C) Quantification of USF1 spots number/cell as in figure 4. USF1 foci are only observed in the presence of *Hp*. (n=150-220 cells/condition). Mann Whitney test: treated or treated/infected *vs* control (**p<0.01; ***p<0.001; ****p<0.0001). Experiments in triplicate with 5-7 fields analysed.

Figure 6. *Hp* inhibits the USF1/p53 complexes in response to a chemical genotoxic stress.

(A) Duolink PLA analysis of USF1/p53 complexes (pink foci), in *Hp*-infected cells either CPT-treated (50nM) or not as described in methods. Nuclei (Hoechst, blue). Experiments in duplicate (5-7 fields analysed). Scale bar: 10µm for each time-point: right panels zoom: fields delimited in red, scale bar 5µm. (B) Quantification of USF1/p53 nuclear interaction. (5-7 fields analyzed). Student t test, CPT-treated and/or infected *vs* control (*p<0.05; **p<0.01; ***p<0.001).

Figure 7. *Hp* infection makes more susceptible gastric cells to a genotoxic stress.

(A) Experimental schedule. MKN45 cells were first infected with *Hp* 7.13 or not, as in figure 3. After 24h, cells were washed 3 times and either treated or not with CPT (50nM) for 24h. (B) IF analysis of USF1 (green) and p53 (red). Nuclei (Hoechst, blue) and phalloidin actin staining (grey). Experiments in duplicate (5-7 fields analysed per condition). Scale bar 5µm.

Figure 8: Schematic representation of the data.

(A) Gastric epithelial cells infected with *Hp* show lower nuclear level of USF1 and p53 and the formation of USF1 foci mainly at the periphery of cells close to membranes. *Hp* infection inhibits USF1 and CPT-induced USF1/p53 complexes in the nuclei. These data support that, in response to a genotoxic stress, the nuclear localization of USF1 is important to maintain p53 in the nucleus to carry out its function. (B) Exacerbation of gastric carcinogenesis due to synergistic effects of *Hp* and environmental DNA damaging factors in chronically-infected individuals. According to our data, the progressive nuclear decrease of USF1 and p53 in *Hp*-positive subjects should lead to further accumulation of DNA damage all lifelong. This supports that *Hp* increases the sensitivity to DNA damaging effects of genotoxic environmental factors, thus promoting the risk of GC.

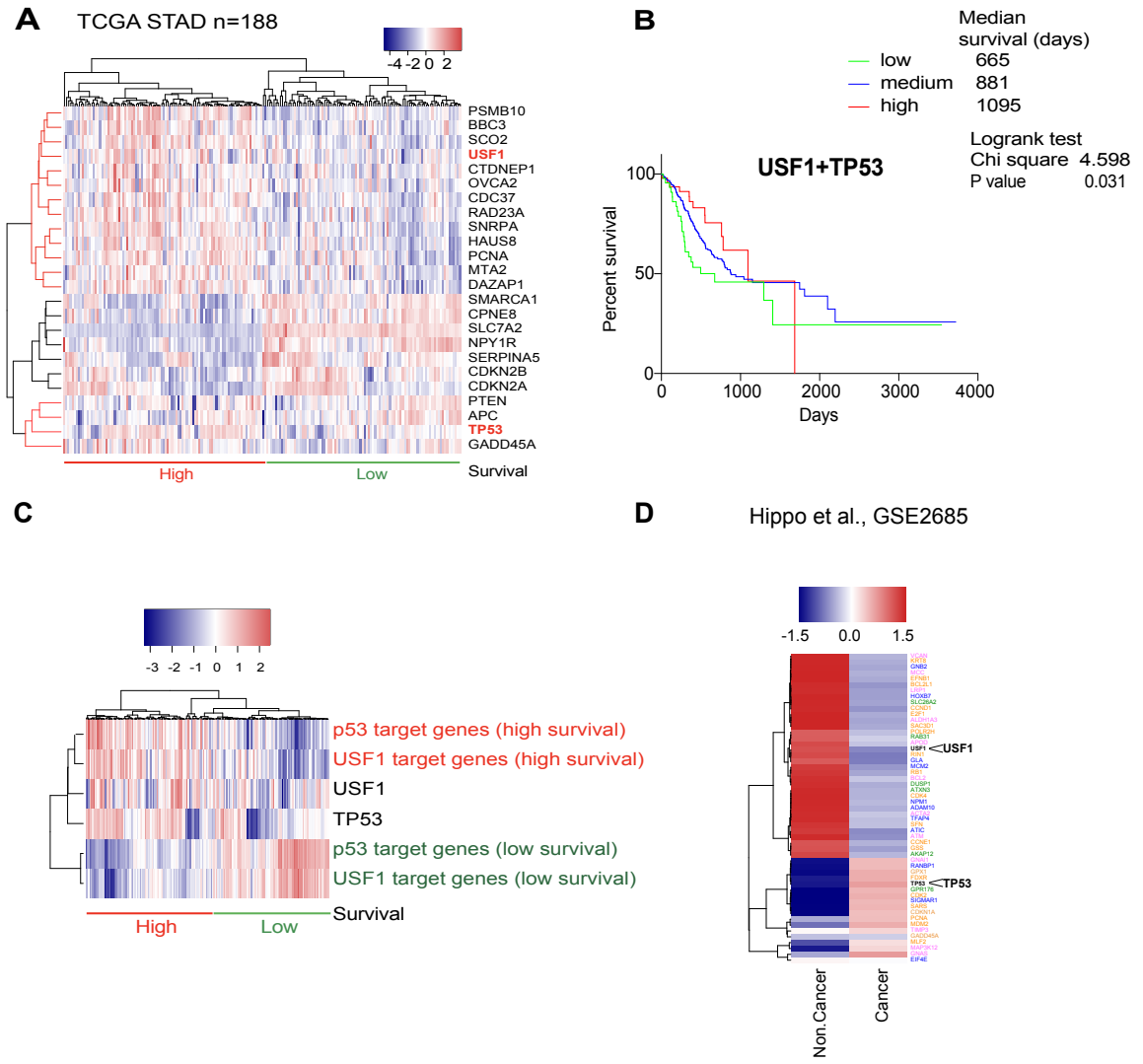
A
TCGA STAD n=188
-4 -2 0 2
PSMB10
BBC3
SCO2
USF1
CTDNEP1
OVCA2
CDC37
RAD23A
SNRPA
HAUS8
PCNA
MTA2
DAZAP1
SMARCA1
CPNE8
SLC7A2
NPY1R
SERPINA5
CDKN2B
CDKN2A
PTEN
APC
TP53
GADD45A
High
Low
Survival
B
Median survival (days)
low 665
medium 881
high 1095
Logrank test
Chi square 4.598
P value 0.031
USF1+TP53
Percent survival
100
50
0
0
1000
2000
3000
4000
Days
C
-3 -2 -1 0 1 2
p53 target genes (high survival)
USF1 target genes (high survival)
USF1
TP53
p53 target genes (low survival)
USF1 target genes (low survival)
High
Low
Survival
D
Hippo et al., GSE2685
-1.5 0.0 1.5
USF1
TP53
Non.Cancer
Cancer
E
Tumor<healthy tissues
Tumor>healthy tissues
H. pylori positive
Fold change Tumor /healthy tissues
****
F
Koeppel et al., GSE55699, Hong et al., E-GEOD-74577
Pearson correlation
r = 0.2885
pvalue = 0.05
log2(fc Hp vs CTR Hong E-GEOD-74577)
log2(fc Hp vs CTR Koeppel GSE55699)

Figure 1

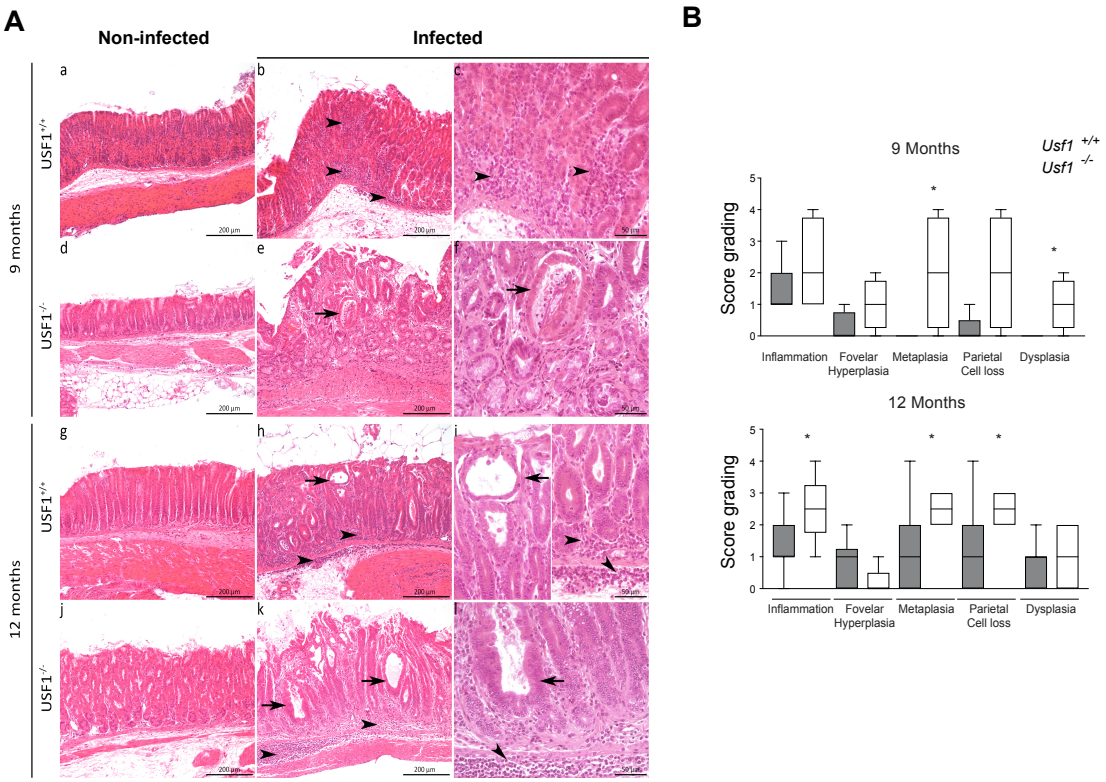
A
Non-infected
Infected
9 months
12 months
USF1+/+
USF1-/-
B
9 Months
Usf1 +/+
Usf1 -/-
Score grading
Inflammation
Fovelar Hyperplasia
Metaplasia
Parietal Cell loss
Dysplasia
12 Months

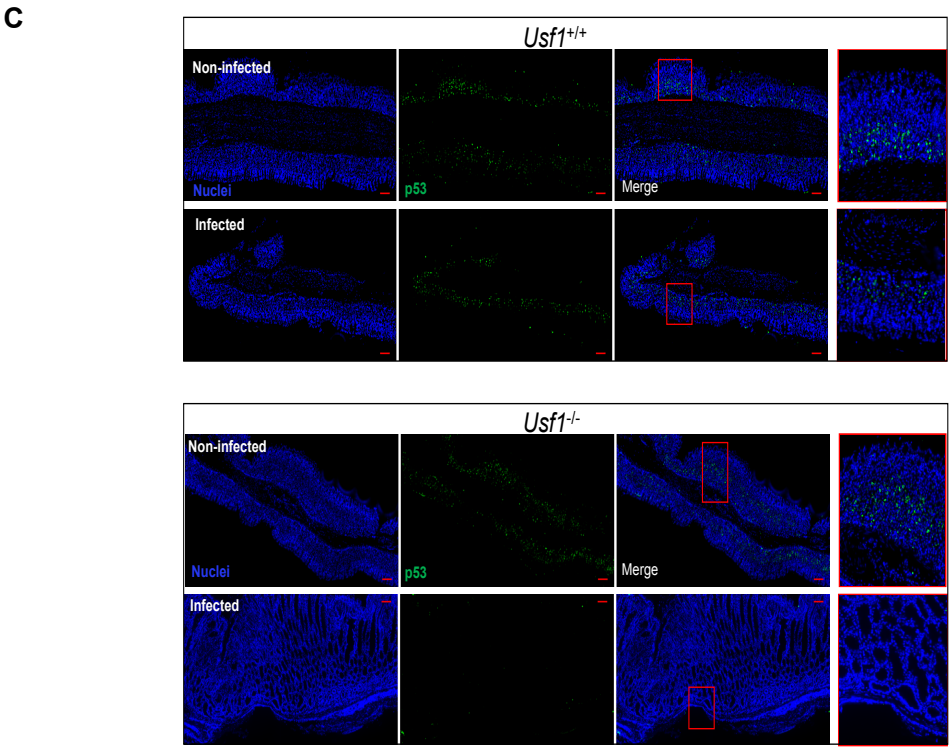
C
Usf1+/+
Non-infected
Infected
Nuclei
p53
Merge
Usf1-/-

Figure 2

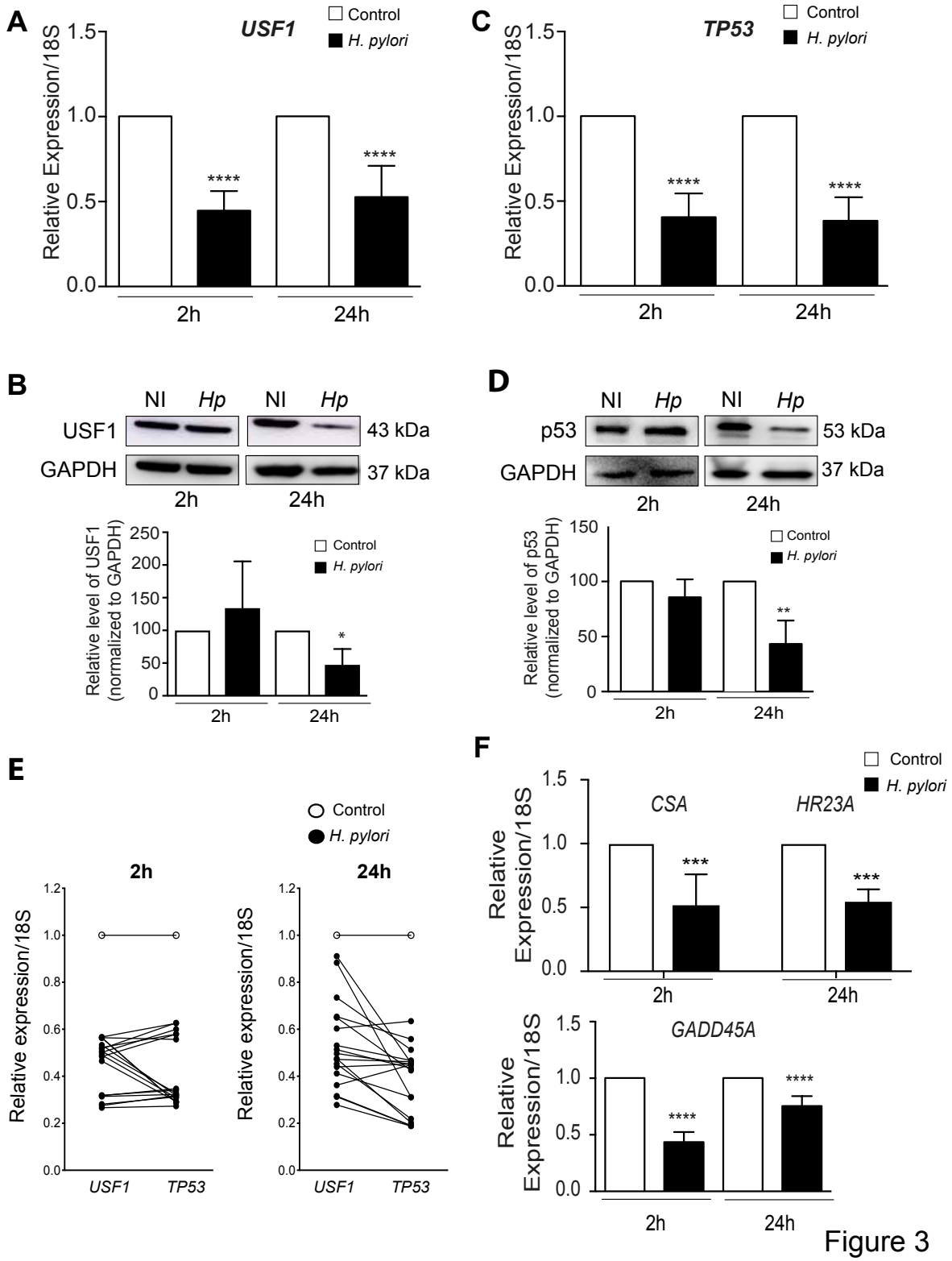
A
USF1
Control
H. pylori
Relative Expression/18S
1.5
1.0
0.5
0.0
****
****
2h
24h
C
TP53
Control
H. pylori
Relative Expression/18S
1.5
1.0
0.5
0.0
****
****
2h
24h
B
NI
Hp
NI
Hp
USF1
43 kDa
GAPDH
37 kDa
2h
24h
Relative level of USF1 (normalized to GAPDH)
250
200
150
100
50
0
Control
H. pylori
*
2h
24h
D
NI
Hp
NI
Hp
p53
53 kDa
GAPDH
37 kDa
2h
24h
Relative level of p53 (normalized to GAPDH)
150
100
50
0
Control
H. pylori
**
2h
24h
E
Control
H. pylori
2h
24h
Relative expression/18S
1.2
1.0
0.8
0.6
0.4
0.2
0.0
USF1
TP53
F
Control
H. pylori
CSA
HR23A
Relative Expression/18S
1.5
1.0
0.5
0.0
***
***
2h
24h
GADD45A
Relative Expression/18S
1.5
1.0
0.5
0.0
****
****
2h
24h

Figure 3

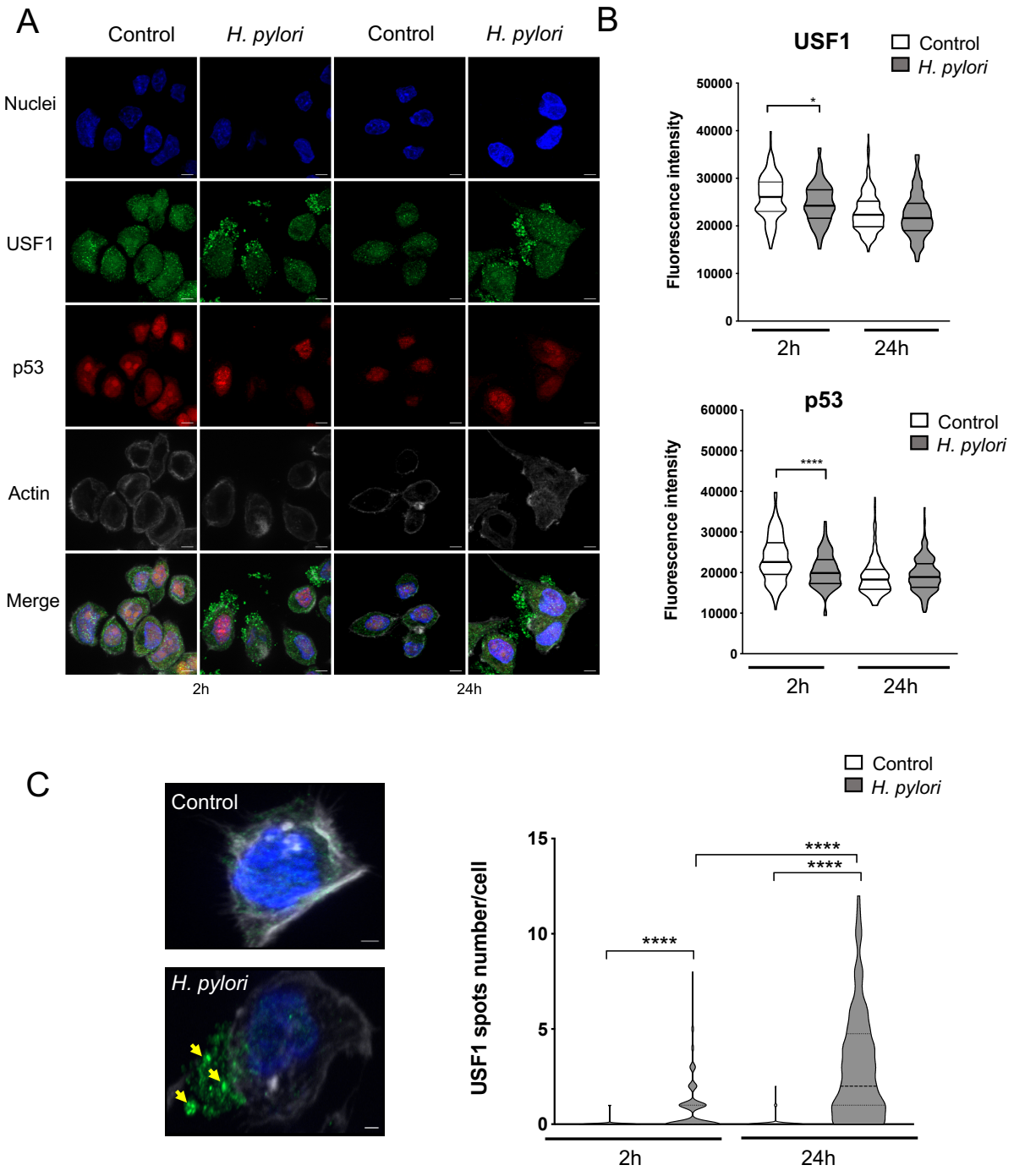
A
Control
H. pylori
Control
H. pylori
Nuclei
USF1
p53
Actin
Merge
2h
24h
B
USF1
Control
H. pylori
Fluorescence intensity
50000
40000
30000
20000
10000
0
*
2h
24h
p53
Control
H. pylori
Fluorescence intensity
60000
50000
40000
30000
20000
10000
0
****
2h
24h
C
Control
H. pylori
Control
H. pylori
USF1 spots number/cell
15
10
5
0
****
****
****
2h
24h

Figure 4

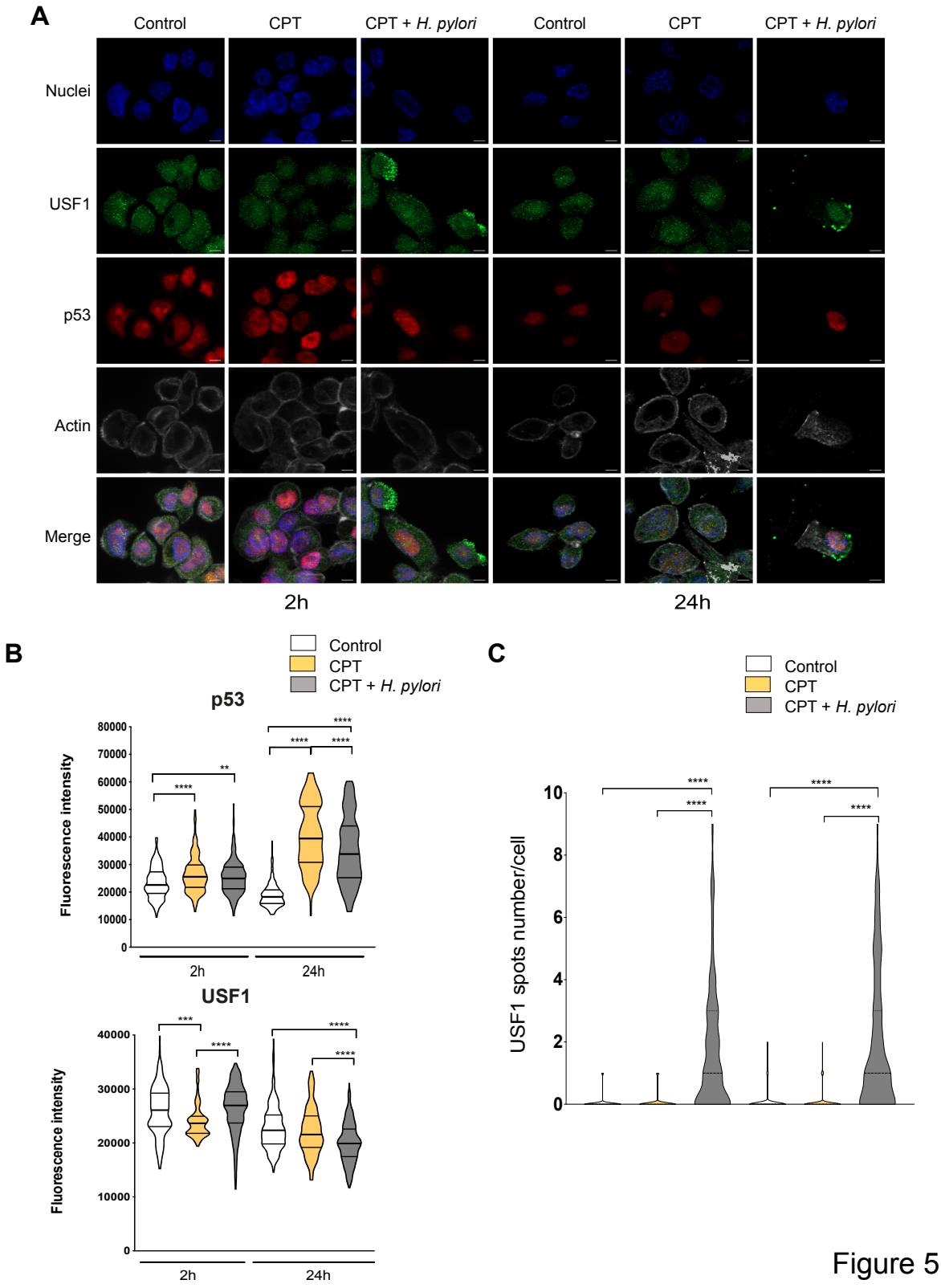
A
Control
CPT
CPT + H. pylori
Control
CPT
CPT + H. pylori
Nuclei
USF1
p53
Actin
Merge
2h
24h
B
Control
CPT
CPT + H. pylori
p53
Fluorescence intensity
80000
70000
60000
50000
40000
30000
20000
10000
0
2h
24h
USF1
Fluorescence intensity
40000
30000
20000
10000
0
2h
24h
C
Control
CPT
CPT + H. pylori
USF1 spots number/cell
10
8
6
4
2
0

Figure 5

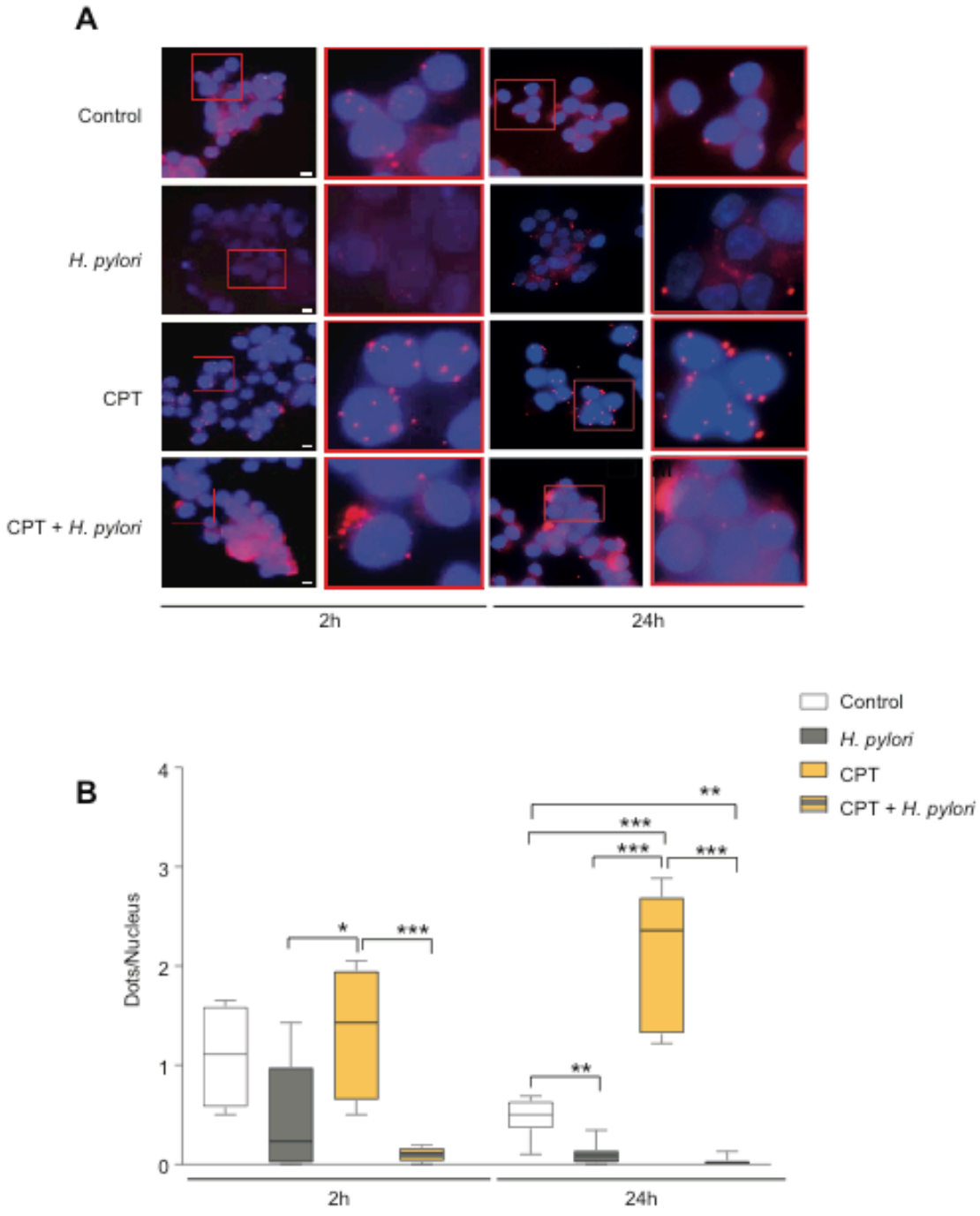
A
Control
H. pylori
CPT
CPT + H. pylori
2h
24h
B
Control
H. pylori
CPT
CPT + H. pylori
Dots/Nucleus
0
1
2
3
4
*
***
**
***
***
***
**
2h
24h

Figure 6

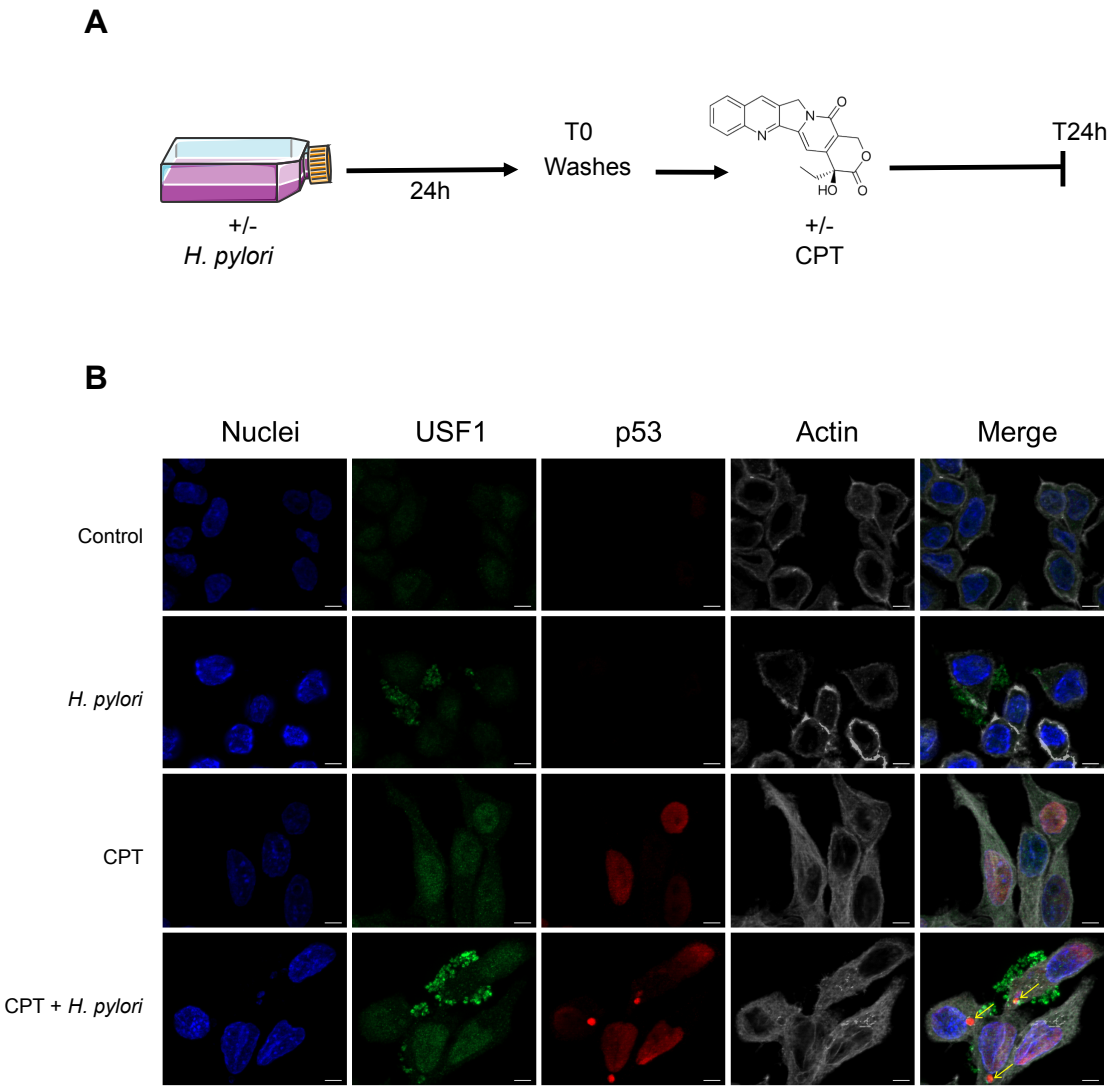
A
T0
Washes
T24h
24h
+/-
H. pylori
+/-
CPT
B
Nuclei
USF1
p53
Actin
Merge
Control
H. pylori
CPT
CPT + H. pylori

Figure 7

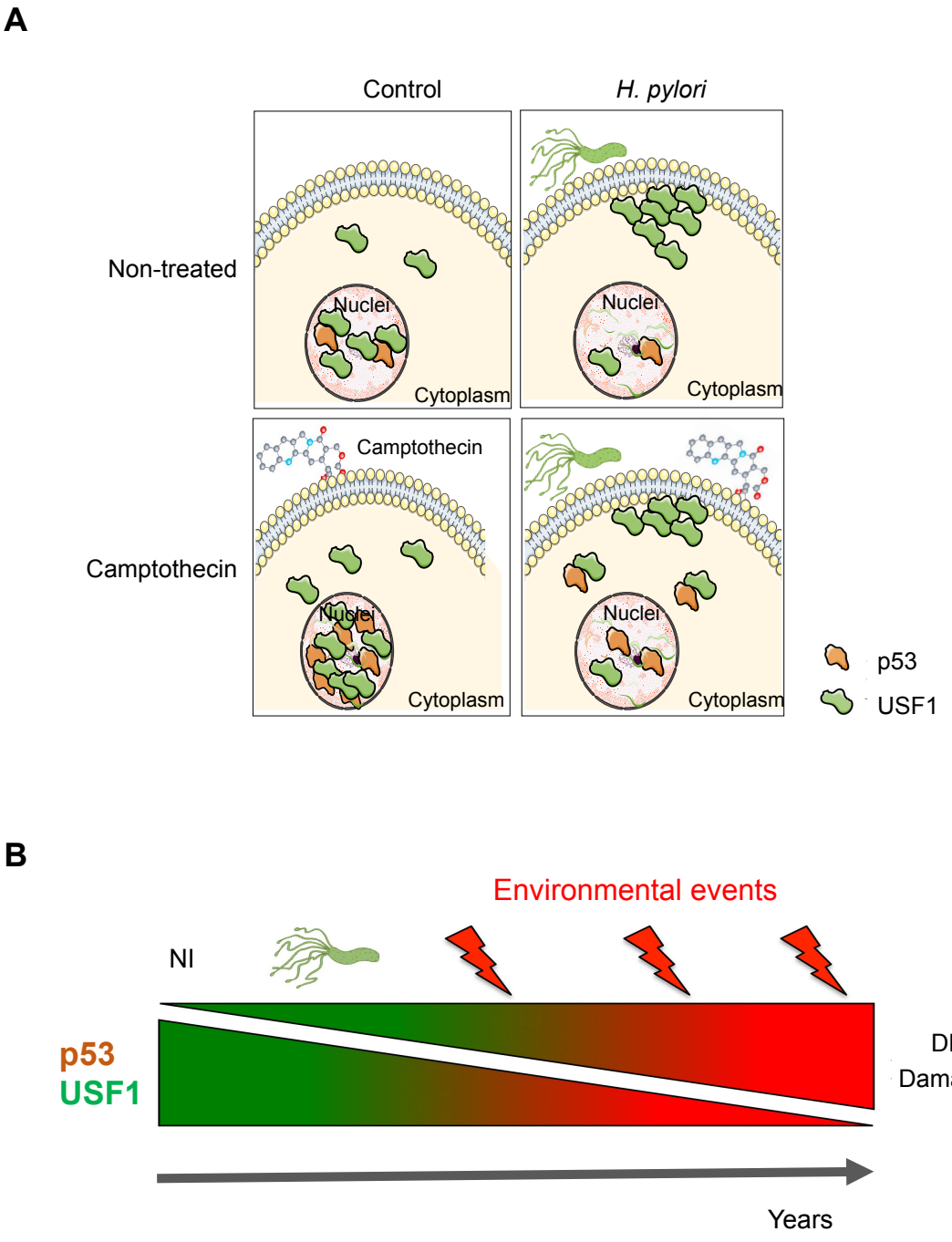
A
Control
H. pylori
Non-treated
Camptothecin
Nuclei
Cytoplasm
Camptothecin
p53
USF1
B
Environmental events
NI
p53
USF1
DNA
Damages
Years

Figure 8

USF1 defect drives p53 degradation during *Helicobacter pylori* infection and accelerates gastric carcinogenesis

Lionel Costa, Sébastien Corre, Valérie Michel, Krysten Le Luel, Julien Fernandes, Jason Ziveri, Grégory Jouvion, Anne Danckaert, Nicolas Mouchet, David Da Silva Barreira, Javier Torres, Margarita Camorlinga-Ponce, Mario Milco D'Elios, Laurence Fiette, Hilde De Reuse, Marie-Dominique Galibert and Eliette Touati.

Supplementary Information

Results

Cytoplasmic aggregation of USF1 is associated with depletion of p53 and gastric intraepithelial neoplasia in INS-GAS mice infected with Hp

To investigate the clinical relevance of *Hp*-induced cytoplasmic accumulation of USF1, we took advantage of the INS-GAS mouse model in which *Hp* accelerates the development of gastric intraepithelial neoplasia[1,2]. As expected, at 6 and 12 months pi mice developed earlier than non-infected, severe gastric hyperplasia, dysplasia and low-grade gastric intraepithelial neoplasia (figure S6A). IF analysis on gastric tissue sections showed a marked cytoplasmic accumulation of USF1 in *Hp*-infected mice (figure S6B), associated to the decrease of p53 levels, as reported at 12 months pi (figure S6C). These results are consistent with *in vitro* data and confirm that USF1 accumulates overtime pi outside the nuclei of *Hp*-infected gastric epithelial cells, concomitantly to p53 depletion.

Material and methods

Bacteria, cell culture and infection

Human gastric epithelial cells, AGS: gastric adenocarcinoma (CRL-1739, ATCC-LGC) and MKN45 used in this study were cultured in RPMI 1640 medium with 10% fetal bovine serum (FBS) and 1% penicillin-streptomycin. *Hp* strains 7.13[3] and SS1[4] were grown at 37°C on 10% blood agar plates under microaerophilic conditions. Bacterial lysates were obtained by passage through a French press and their proteins concentration determined by Dc Protein assay (Bio-Rad, Hercules, CA, USA).

Cells preparation, immunostaining and microscopy

Cells were fixed on slides with 4% paraformaldehyde (PFA) in 0.1M Phosphate buffer (15735-60S, Electron Microscopy Sciences) for 15min at room temperature (RT), incubated 1h at RT in quenching buffer (NH_4Cl 50mM, PBS). The primary antibodies used were, anti-USF1 (Ab167693, Abcam; 1/100), anti-p53 (FL-393) (sc-6243, Santa Cruz Biotechnology, CA, USA; 1/200) and anti-γH2AX (p-Ser139) (NB100-384, Novus Biologicals 1/2500). The nuclear DNA was stained with NucBlue® Live ReadyProbes® Reagent ((R37605), Thermo Fisher Scientific, USA) and actin stained with Alexa Fluor® 647 Phalloidin (A22287, Thermo Fisher Scientific, USA, 1/100). Sample images were acquired with an Inverted Widefield Microscope Axio Observer Z1 equipped with Apotome grid (Carl Zeiss, Germany) with a Plan-Apochromat 63x1.40 Oil M27 objective. In the case of MMS and H_2O_2 experiments (Figures S8 to S10), image acquisition was performed using a spinning disk SP8 microscope. Random field images were acquired as 211.30 × 211.30 μm^2 with a depth of 100µm at 7µm increment.

Image processing and immunofluorescence quantification

After acquisition, a maximum of intensity projection processing from images were done using automated free plugins of the imageJ v1.50 software interface[5]. Image analysis was carried out using Acapella software (version 2.7, PerkinElmer Life Sciences). The script was subdivided into three object subroutines segmenting successively the nucleus, the cytoplasm, and USF1 spots within the cytoplasm and membrane surrounding area of each cell. First the cell regions are determined by nuclei and cytoplasm detection library modules using the appropriated channel images. Spots corresponding to USF1 foci are detected in the cytoplasm body areas using Alexa Fluor AF488 channel. The parameters of the detected spots, (e.g. number, intensity) are added to the cell object list. A number of numerical output values is generated. Spot candidates are detected as local intensity maximums within cytoplasm. Thereupon the

spots are selected by contrast and intensity parameters. For each condition, 5 microscopic fields were analysed and n=150 to 220 cells quantified.

Analysis of gene expression

Human gastric epithelial cells MKN45 were infected with the *Hp* strains at a multiplicity of infection (MOI) of 100 bacteria per cell for 2 and 24h.

Total RNA was isolated from MKN45 cells, from mice stomach or from human gastric biopsies using the RNeasy Mini Kit (Qiagen). It was reverse-transcribed using Superscript® III Reverse transcriptase (Invitrogen) and amplified with Power Sybr Green PCR Master Mix (Applied Biosystems) using the StepOne^{TM} Plus Real-Time PCR system (Applied Biosystems). Primers used for each gene are listed in the table S2. Target genes were normalized according to the *18SrRNA* genes for analysis in MKN45 cells. The analysis of *USF1* gene expression in human gastric biopsies was performed using the Real-Time PCR TaqMan gene expression kit (Applied Biosystems), normalized according to the *18SrRNA* gene, with commercial primers reported in the supplementary table S1. Amplification PCR consisted in 40 cycles of 15 seconds at 95°C and 1 min 60°C. Data were analysed by StepOne Plus RT-PCR software v2.1. Experiments were performed in triplicate.

Table S1: List of human primers used for the quantification of gene expression

Gene name	Primer
FH1_USF1	TCACAAAGAATTGACCAGTG
RH1_USF1	GACGCACTATACTTACTTCC
FH1_TP53	ACCTATGGAAACTACTTCCTG
RH1_TP53	ACCATTGTTCAATATCGTCC
hCSA-F	GTTCCAATGGAGAAAACACACTT
hCSA-R	CCATATGGTACAAAAACAAATTCTGA
hHR23A-F	GTCACCATCACGCTCAAAAC
hHR23A-R	CTATCTTCTCCTTTAGCACCTTCAC
hGADD45a-F	TCAGCGCACGATCACTGTC
GADD45a-R	CCAGCAGGCACAACACCAC
hp21/CDKN1A-F	CTGGAGACTCTCAGGGTCGAA
hp21/CDKN1A-R	CGGCGTTTGGAGTGGTAGA
FH1_RN18S1	ATCGGGGATTGCAATTATTC
RH1_RN18S1	CTCACTAAACCATCCAATCG
FH1_TBP	GCCAAGAGTGAAGAACAG
RH1_TBP	GAAGTCCAAGAACTTAGCTG

Primers for TaqMan® Gene Expression Assays
(Applied Biosystems, Foster City, CA)

Gene name	Primer
Human USF1	Hs00982868_m1
Human 18S	Hs99999901_s1

Analysis of protein levels by Western blot

After co-culture with *Hp*, cells were lysed in NP-40 buffer containing protease inhibitors; 30 µg per lane was separated on a 12 % Mini-PROTEAN® TGX Stain-Free™ Precast Gels (BioRad) and transferred onto Trans-Blot® Turbo™ Midi PVDF Transfer Packs using a Trans-Blot® Turbo™ Transfer System (BioRad). USF1 (EPR6430 ab125020 ; Abcam, dilution 1/5000), USF2 antibodies ((C-20) Ref sc-862 ; Santa Cruz Biotechnology, CA,USA; dilution 1/200), GAPDH ((FL-335) sc-05778, Santa Cruz Biotechnology, CA,USA; 1/100), p53 ((FL-393) sc-6243, Santa Cruz Biotechnology, CA,USA; dilution 1/100)**,** β-Actin ((BA3R) (MA5-15739), ThermoFisher Scientific, USA, dilution 1/5000) were used followed by a goat anti-rabbit IgG-HRP (sc-2054, Santa Cruz Biotechnology, CA,USA; 1/10000) or Anti-Mouse IgG

HRP Conjugate ((W402B), Promega, Dilution 1/5000). Detection was performed using the SuperSignal™ West Femto Maximum Sensitivity Substrate (ThermoFisher Scientific, USA) and a ChemiDoc XRS (Bio-Rad). Western blot data were quantified by densitometry using Image Lab software (Bio-Rad).

Analysis of protein complexes by proximity ligation assay (PLA)

MKN45 Cells, grown on glass coverslips, were fixed with 4% PFA in 0.1M Phosphate buffer (15735-60S, Electron Microscopy Sciences) for 15min at RT and PLA was performed using the kits ((DUO92007) Duolink® in Situ Detection Reagent Orange, (DUO92001) Duolink® in Situ PLA® Probe Anti-Mouse PLUS, (DUO92005) Duolink® in Situ PLA® Probe Anti-Rabbit MINUS, Sigma) according to the manufacturer's protocol. After blocking, the reaction with primary antibodies, rabbit anti-USF1 (C20, sc-229, Santa Cruz Biotechnology, CA, USA, 1/100) and mouse anti-p53 (1C12, #2524, Cell Signaling Technologies, MA, USA, 1/100) was performed. Protein-protein interactions are revealed with species-specific secondary antibodies conjugated to complementary oligonucleotide allowing ligation and amplification of complementary DNA if the two proteins are in close proximity[6].

In silico analyses

Heatmaps were generated with R-packages heatmap3[7]. Gene Set Enrichment Analysis were performed using GSEA 3.0 tool from the Broad Institute software (http://software.broadinstitute.org/cancer/software/gsea)[8]. STAD TCGA expression data were obtained using cBioPortal (https://www.cbioportal.org/)[9].

Expression data were obtained from GSE2685[10], GSE55699[11], .E-GEOD-74577 (Hong et al) (https://www.ebi.ac.uk/arrayexpress/experiments/), GSE5081[12] and E-MEXP-1135[13] (https://www.ebi.ac.uk/arrayexpress/experiments/E-MEXP-1135/).

Gene set enrichment analysis (GSEA version 3.0)[9] was performed by ranking TCGA (STAD, low survival versus high survival for gastric cancer patients) genes based on their cZ-score as metric. Different ranked lists were used including low (top 25%) versus high (top 25%) survival for gastric cancer patients (STAD, n=188). The following gene signatures were analyzed for enrichment: KEGG pathways gene sets, **using p53 target genes (FISCHER_DIRECT_P53_TARGETS_META_ANALYSIS Gene set, n=298) or using USF putative target genes (USF_01 Gene set, n=256) (http://software.broadinstitute.org/gsea/msigdb).**

Genotyping of INS-GAS mice

Usf1$^{-/-}$[14] and *Usf1*$^{+/+}$ wild-type (WT) mice (C57BL/6j 129SV) previously provided by S. Vaulont (Institut Cochin, Paris, France) were maintained under specific pathogen free (SPF) conditions and reproduced in the animal facility (University of Rennes) (ARCHE-BIOSIT UMS 34380 (N°A35 23840). The USF1 deletion in *Usf1*$^{-/-}$ mice was validated by PCR using the following primers: USF1-Int2-F (WT or KO): TTGGGAACCATGTTACGAGG, USF1-IRES-R (KO): TACCCGGGGATCCTCTAGAG, and USF1-Int4-R (WT): ACAGCTACTCCTCCAAGCCAC.

INS-GAS mice[1,2] (FVB/N genetic background) were breeded at the animal facility (Institut Pasteur, Paris), from couples provided by TC Wang (Columbia University College, NY, USA). The INS-GAS trans-gene[2] was confirmed in all mice by tail genotyping using the PCR primers: Forward: 5' TGATCTTTGCACTGGCTCTG3' and Reverse: 5'TCCATCCATCCATAGGCTTC3'.

Hp infection of mice

For both mouse models, 14 5-6 weeks-old male mice were orally inoculated with *Hp* SS1 (10^8

colony-forming units (cfu)/100µl) at days 1 and 3; non-infected mice (n=14) received peptone broth. After 6 (9 months for *Usf1*$^{-/-}$) and 12 months mice were sacrificed (n=7/group). Gastric tissues were collected for histopathological and immunofluorescence analysis as already reported[15]. *Hp* gastric colonization was evaluated as previously described[16].

Histopathology analysis of gastric lesions

Stomach samples from non-infected and infected mice were fixed in RCL2® (Alphelys, France) and embedded in low-melting-point paraffin wax (Poly Ethylene Glycol Distearate; Sigma, USA). 4 µm-thick sections were stained by hematoxylin and eosin treatment (H&E) and examined blindly for histopathologic lesions. Histologic alterations (i.e. inflammation, ulceration, foveolar hyperplasia, intestinal metaplasia, parietal cell loss, dysplastic changes of the gastric mucosa and herniation), which were semi-quantitatively evaluated based on a scoring system with five severity grades (1: minimal, 2: mild, 3: moderate, 4: marked and 5: severe) were characterized as previously described[15].

Immunofluorescence on gastric tissues from mice

Gastric tissue sections (4 µm) were taken from infected and control mice were dewaxed (5min (2x) Xylene, 2min (2x) Ethanol 100%), rehydrated 5min in PBS-1X, blocked 1h in PBS-1X + 3% BSA + 0.4% Triton X-100 at room temperature (RT). Then incubated with the primary antibody anti-USF1 ((C-20) sc-229, Santa Cruz Biotechnology, CA, USA; dilution 1/100), anti-p53 monoclonal Antibody (SP5) MA5-14516, ThermoFisher Scientific, USA; dilution 1/100) in PBS-1X, 0.4% Triton X-100 and 3% BSA overnight at 4°C. A secondary Goat anti-rabbit IgG (H+L) Highly Cross-Adsorbed Secondary Antibody, Alexa Fluor 546 ((A11035), ThermoFisher Scientific, USA, dilution 1/400) in PBS-1X + 0,4% Triton X-100 + 3% BSA was applied. The nuclear DNA was stained with NucBlue® Live ReadyProbes® Reagent

((R37605), ThermoFisher Scientific, USA). USF1 staining were observed with an Inverted widefield Microscope Axio Observer ZI equipped with Apotome grid (Carl Zeiss, Germany) using a 63x/1.4 oil immersion objective. p53 staining were acquired at 20X with Axio scan Z1 Zeiss® by using Zen software.

References

1. Fox J, Rogers A, Ihrig M, *et al. Helicobacter pylori* associated gastric cancer in INS-GAS mice is gender specific. *Can Res* 2003;63:942-50.
2. Wang T, Dangler C, Chen D, et al. Synergistic interaction between hypergastrinemia and Helicobacter infection in a mouse model of gastric cancer. *Gastroenterology* 2000;118:36-47.
3. Franco AT, Israel DA, Washington MK, *et al.* Activation of beta-catenin by carcinogenic *Helicobacter pylori. Proc Natl Acad Sci U S A* 2005;102:10646-51.
4. Lee A, O'Rourke J, Ungria M, *et al.* A standardized mouse model of *Helicobacter pylori* infection : introducing the Sydney strain. *Gastroenterology* 1997;112:1386-1397.
5. Schindelin J, Arganda-Carreras I, Frise E, *et al.* Fiji: an open-source platform for biological-image analysis. *Nat Methods* 2012;9:676-82.
6. Soderberg O, Gullberg M, Jarvius M, *et al.* Direct observation of individual endogenous protein complexes in situ by proximity ligation. *Nat Methods* 2006;3:995-1000.
7. Zhao S, Guo Y, Sheng Q, *et al.* Advanced heat map and clustering analysis using heatmap3. *Biomed Res Int* 2014;2014:986048.
8. Subramanian A, Tamayo P, Mootha VK, *et al.* Gene set enrichment analysis: a knowledge-based approach for interpreting genome-wide expression profiles. *Proc Natl Acad Sci USA* 2005;102:15545-50.
9. Gao J, Aksoy BA, Dogrusoz U, *et al.* Integrative analysis of complex cancer genomics and clinical profiles using the cBioPortal. *Sci Signal* 2013;6:l1.
10. Hippo Y, Taniguchi H, Tsutsumi S, *et al.* Global gene expression analysis of gastric cancer by oligonucleotide microarrays. *Cancer Res* 2002;62:233-40.
11. Koeppel M, Garcia-Alcalde F, Glowinski F, *et al. Helicobacter pylori* Infection Causes Characteristic DNA Damage Patterns in Human Cells. *Cell Rep* 2015;11:1703-1713.

12. Galamb O, Gyorffy B, Sipos F, *et al. Helicobacter pylori* and antrum erosion-specific gene expression patterns: the discriminative role of CXCL13 and VCAM1 transcripts. *Helicobacter* 2008;13:112-26.
13. Vivas JR, Regnault B, Michel V, *et al.* Interferon gamma-signature transcript profiling and IL-23 upregulation in response to *Helicobacter pylori* infection. *Int J Immunopathol Pharmacol* 2008;21:515-26.
14. Vallet VS, Casado M, Henrion AA, et al. Differential roles of upstream stimulatory factors 1 and 2 in the transcriptional response of liver genes to glucose. *J Biol Chem* 1998;273:20175-9.
15. Touati E, Michel V, Thiberge J, *et al.* Chronic *Helicobacter pylori* infections induce gastric mutations in mice. *Gastroenterology* 2003;124:1408-1419.
16. Ferrero RL, Thiberge JM, Huerre M, *et al.* Immune responses of specific-pathogen-free mice to chronic *Helicobacter pylori* (strain SS1) infection. *Infect Immun* 1998;66:1349-55.
17. Bussière FI, Michel V, Memet S, *et al. H. pylori*-induced promoter hypermethylation downregulates USF1 and USF2 transcription factor gene expression. *Cell Microbiol* 2010;12:1124-33

Legend of supplementary figures

Figure S1. Involvement of p53 pathway and USF1 targets in gastric carcinogenesis.

(A) Survival curve for GC patients (TCGA, STAD n=188) according to *SLC7A2* mRNA level, a most discriminant gene (25% top low: blue or 25% to high: red). (B) Survival curve for GC patients according to *USF1* and *TP53* mRNA levels (low: green, medium: blue or high: red). (C) Correlation of *USF1* and *TP53* mRNA level expression from the stomach of gastric adenocarcinoma patients (TCGA, Provisional n=478; cBioPortal: https://www.cbioportal.org/). Each symbol corresponds to one patient. (D) Expression Heatmap, in GC patients associated with both low and high survival, and depicting median mRNA expression of genes specific to the different KEGG pathways (KEGG gene sets), and that have been shown to be enriched after Gene Set Enrichment Analysis (GSEA, broadinstitute), (E-F) Gene Set Enrichment Analysis (GSEA, broadinstitute) in GC patients associated with both low and high survival, (E) using p53 target genes (FISCHER_DIRECT_P53_TARGETS_META_ANALYSIS Gene set, n=298) or (F) using USF putative target genes (USF_01 Gene set, n=256). (G) Relative *USF1* gene expression in gastric biopsies from GC patients (n=34) measured by qRT-PCR (tumoral *vs* adjacent tissue), comparison between *Hp*-positive and *Hp*-negative patients. A trend for a lower *USF1* gene expression in the tumor-tissue *vs* adjacent-tissue is observed in *Hp*-positive patients compared to *Hp*-negative patients.(Mann-Whitney test*; Hp*-positive vs *Hp*-negative).

Figure S2. p53 and USF1 loss correlate with the deregulation of their target genes and low survival of GC patients

Expression Heatmap depicting mRNA expression of top 50 p53-target genes (Fisher_direct_p53_targets_meta_analysis, GSEA) and top 50 putative USF1-target genes (Genes having at least one occurrence of the transcription factor binding site V$USF_01 (v7.4 TRANSFAC) in the regions spanning up to 4 kb around their transcription starting sites,

GSEA), that have been significantly enriched in both low and high survival GC population. p53 and USF1 target genes (p53-targets: orange and pink; USF1-targets: blue and green; common targets: black), previously correlated with low (pink and green) or high survival (orange and blue) using expression data from Hippo and coll[10] comparing noncancerous and cancerous tissues (Figure 1D).

Figure S3. Lack of USF1 leads to inhibition of the expression of p53- and USF1-target genes in *Hp*-infected *Usf1*$^{-/-}$ mice.

(A) Expression Heatmap depicting mRNA expression of p53 and USF1 target genes previously correlated with low or high survival (figure 1A-C), using data from GSE5081 (Galamb and coll)**[12]** for gastric biopsies of patients with *Hp*-positive and *Hp*-negative antrum erosions (E+) (8/8) and adjacent normal mucosae (E^{-}) (8/8) (p53-targets: orange and pink; USF1-targets: blue and green; common: black)**.** (B) Log-fold enrichment for p53 and USF1 target genes expression in chronically *Hp*SSI infected and non-infected mice after 12 months from E-MEXP-1135 (Vivas and coll)**[13]** (C) Gastric colonization measured from stomach fragments isolated from *Usf1*$^{+/+}$ and *Usf1*$^{-/-}$ mice sacrificed after 9 and 12 months of infection with *Hp*SS1. The non-infected control groups are not colonized and are not reported. The number of colonies forming unit (cfu) was determined as previously described[16]. (D) Expression of the p53-targets *GADD45, CDKN1A*, *PCNA*; *CSA*, *HR23A* genes related to the NER pathway regulated by both USF1 and p53, and *RAB31* an USF1-target measured by RT-qPCR, on RNA isolated from the stomach of *Usf1*$^{-/-}$ and *Usf1*$^{+/+}$ mice infected for 12 months as described in the supplementary methods. The absence of USF1, in *Usf1*$^{-/-}$ mice, leads to the inhibition of the expression of *HR23A* and *CSB*, as well as *GADD45*, *PCNA* and *RAB31* gene expression in infected mice. Mean±SD. Student t test; infected *vs* non-infected (*p<0.05; **p<0.01; ***p<0.001; ****p<0.0001).

Figure S4. *Hp* total extracts inhibit USF1 and p53 levels and impair host DNA repair function.

Human adenocarcinoma gastric epithelial cells MKN45 cells were treated with total extracts of the strain *Hp*7.13 at 50µg/ml and 100µg/ml for 2h and 24h. Control cells were not treated. (A) *USF1,* (C) *TP53* and (E) *CSA* and *HR23A* mRNA were quantified by RT-qPCR. (B) USF1 (D) p53 and GAPDH (loading control) western blots analysis. Under this condition, an inhibition of *USF1* gene expression was observed, as well as protein level at 24h pi, in agreement with a cag-PAI-independent regulation, as we previously observed[17]. The *TP53* gene expression and protein level are also down-regulated, as *CSA* and *HR23A*. The histogram below corresponds to the immunoblot quantification normalized to GAPDH as described in the methods section. Mean±SD, n=3. Student t test; infected *vs* non-infected (** $p<0.01$; ****$p<0.0001$). (F) Analysis of γH2AX levels indicating the presence of DSB in MKN45 cells infected with *Hp* 7.13 at MOI 100:1 for 2h and 24h, γH2AX immunofluorescence staining (red) and nuclei (Hoechst, blue). Experiments have been done in duplicate with 5 to 7 microscopic fields analysed for each condition. Scale bar: 2µm.

Figure S5. The *Hp* strain SS1 used to colonize the mice stomach also inhibits USF1 and p53 level *in vitro*.

Human adenocarcinoma gastric epithelial cells MKN45 cells were infected with the *Hp* strain SS1 at MOI 100:1 for 2h and 24h. Control cells were not infected. (A) *USF1, (C) TP53* mRNA were quantified by RT-qPCR and (B) USF1, (D) p53 protein levels analyzed by western blot. *Hp*SS1 also inhibits USF1 and p53 gene expression and protein level, but at a lower extent compared to *Hp*7.13 (see figure 3). The histogram below corresponds to the immunoblot quantification normalized to GAPDH as described in material and methods. Mean±SD, n=3. Student t test; infected *vs* non-infected (**$p<0.01$; *** $p<0.001$).

Figure S6. *Hp* leads to USF1 cytoplasmic accumulation in the gastric mucosa of INS-GAS mice and induces gastric cancer lesions.

Mice were orally infected with *Hp* SS1 for 6 and 12 months, and gastric lesions compared to non-infected mice. (A) Representative gastric histological changes in *Hp*-infected mice (b, d) and non-infected (NI) (a, c) after 6 (a, b) and 12 months (c, d) on H&E stained paraffin sections. Scale bar: 500 μm. Infected mice at 6 months pi (b) show hyperplastic and metaplastic lesions compared to controls (a). At 12 months, infected-mice (d) display more severe hyperplasia and dysplasia than uninfected-mice (c) with low-grade gastric intraepithelial neoplasia, as defined by dysplasia and herniation into the sub-mucosa. (B) USF1 IF (green) and nuclei (Hoechst, blue) in gastric tissue sections after 6 (left part) and 12 months (right part), showing a predominant USF1 staining and accumulation in the cytoplasm of gastric cells, observed concomitantly with the presence of gastric intraepithelial neoplasia. Scale bar, 20μm. (C) p53 immunostaining (green) in gastric tissue section from *Hp*-infected and non-infected INS-GAS mice after 12 months. Also in this genetic background and concomitantly to the development of gastric intraepithelial neoplasia, *Hp* inhibits p53 levels, in parallel to USF1 delocalisation.

Figure S7. Induction of DSB in CPT-treated cells infected with *Hp*.

IF analysis of γH2AX levels indicating the presence of DSB in MKN45 cells treated with CPT (50nM) and infected or not with *Hp*7.13 at MOI 100:1 for 24h. γH2AX (red) and nuclei (Hoechst, blue). Experiments have been done in duplicate with 5 to 7 microscopic fields analysed for each condition.

Figure S8. The induction of USF1 foci is *Hp*-dependent and not observed in MMS-treated cells

(A) IF analysis of USF1 and p53 levels and localization, in MKN45 cells treated or not with MMS (1mM) and infected with *Hp* 7.13 or not-infected, for 2 and 24h. p53 (red), USF1 (green), nuclei (Hoechst, blue) and phalloidin actin staining (grey). The delocalization and accumulation of USF1 are specifically observed in the cytoplasm and membrane surrounding area of *Hp*-infected/MMS-treated cells. Scale bar 5µm. (B) Quantification of USF1 and p53 cellular IF intensity. IF intensity measured for USF1 and p53 is decreased in MMS-treated cells and *Hp* infected (n=150-220 cells/condition). (C) Quantification of USF1 spots number/cell as in figure 5, showing that USF1 foci are only observed in the presence of *Hp* as in the case of CPT±*Hp* cells (see figure 5). (n=150-220 cells/condition), Mann-Whitney test, treated/infected *vs* control ((*p<0.05; ****p<0.0001). Experiments in triplicate with 5-7 fields analysed.

Figure S9. The induction of USF1 foci is *Hp*-dependent and not observed in H_2O_2-treated cells

(A) IF analysis of USF1 and p53 levels and localization, in MKN45 cells treated or not with H_2O_2 (1mM) and infected with *Hp* 7.13 for 2 and 24h. p53 (red), USF1 (green), nuclei (Hoechst, blue) and phalloidin actin staining (grey). The delocalization and accumulation of USF1 are specifically observed in the cytoplasm and membrane surrounding area of *Hp*-infected/H_2O_2-treated cells. Scale bar 5µm. (B) Quantification of USF1 and p53 cellular IF intensity which is decreased in H_2O_2-treated cells and *Hp* infected, as previously observed in CPT (or MMS)-treated/infected cells (n=150-220 cells/condition). (C) Quantification of USF1 spots number/cell as in figure 3. A significant increase of USF1 foci is only observed in the presence of *Hp*. (n=150-220 cells/condition), Mann-Whitney test, treated/infected *vs* control (****p<0.0001). Experiments in triplicate with 5-7 fields analysed.

Figure S10. The formation of USF1 foci is maintained in previously *Hp*-infected cells, whatever the genotoxic stress underwent by cells.

MKN45 cells were first infected with *Hp* 7.13 or not, as described in the supplementary information. After 24h, cells were washed 3 times and either treated or not with (A) MMS (1mM) and (B) H_2O_2 (1mM) for 24h as in figure 7A. IF analysis of USF1 (green) and p53 (red). Nuclei (Hoechst, blue) and phalloidin actin staining (grey). In both cases, either MMS or H_2O_2 post-infection treatment, USF1 foci are observed in the peripheral/cytoplasmic parts of cells, as observed in CPT-treated cells 24h post-*Hp* infection (see figure 7B). Scale bar 5µm.

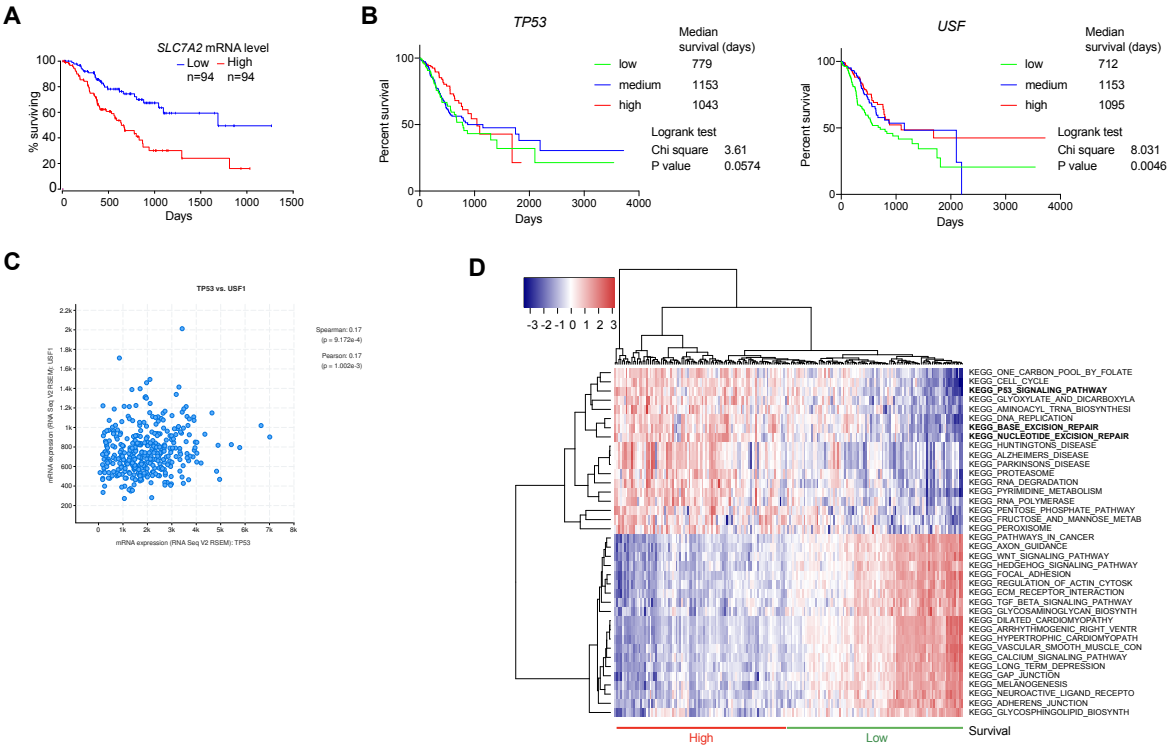

E Genes directly bound and regulated by TP53 (GSEA)

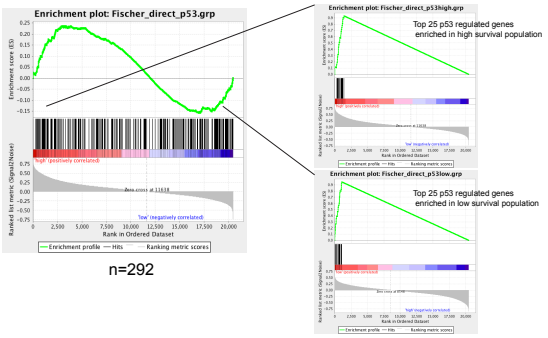

F Genes having at least one occurence of the transcription factor binding site V$USF_01 (v7.4 TRANSFAC) in the regions spanning up to 4 kb around their transcription starting sites.

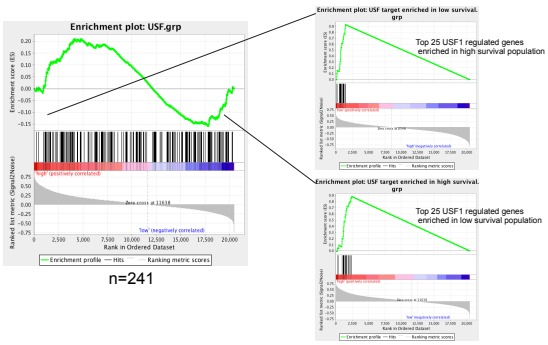

G

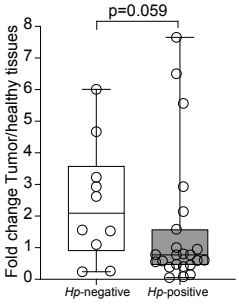

Figure S1

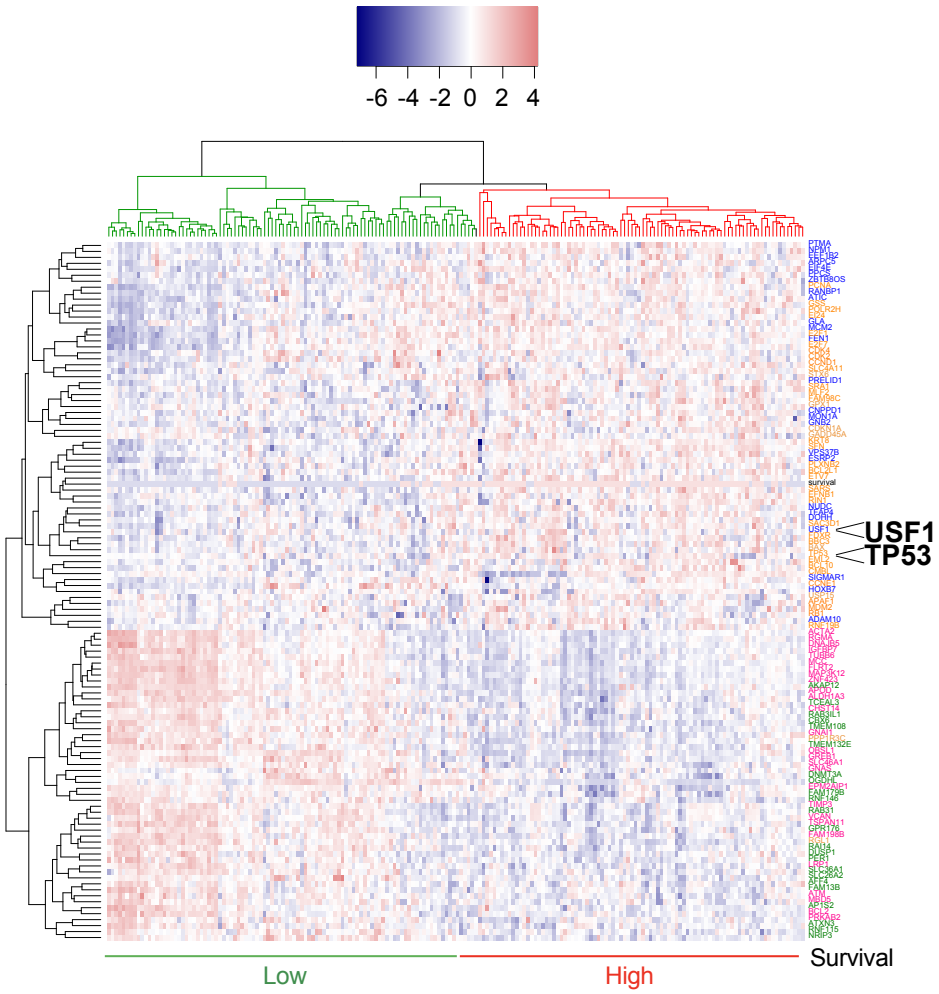

Figure S2

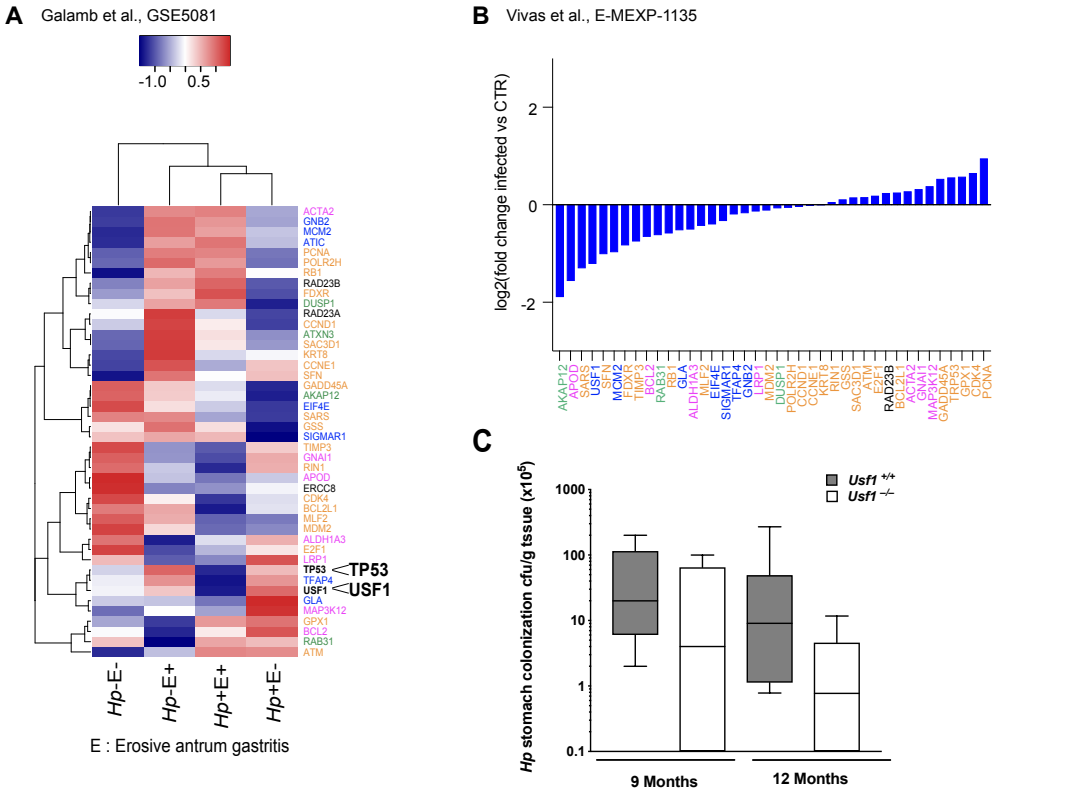
A
Galamb et al., GSE5081
-1.0
0.5
ACTA2
GNB2
MCM2
ATIC
PCNA
POLR2H
RB1
RAD23B
FDXR
DUSP1
RAD23A
CCND1
ATXN3
SACS
KRT8
CCNE1
SFN
GADD45A
AKAP12
EIF4E
SARS
GSS
SIGMAR1
TIMP3
GNAI1
RIN1
APOD
ERCC8
CDK4
BCL2L1
MLF2
MDM2
ALDH1A3
E2F1
LRP1
TP53
TFAP4
USF1
GLA
MAP3K12
GPX1
BCL2
RAB31
ATM
TP53
USF1
Hp-E-
Hp-E+
Hp+E+
Hp+E-
E : Erosive antrum gastritis
B
Vivas et al., E-MEXP-1135
log2(fold change infected vs CTR)
2
0
-2
AKAP12
APOD
SARS
USF1
SFN
MCM2
FDXR
TIMP3
BCL2
RAB31
RB1
GLA
ALDH1A3
MLF2
EIF4E
SIGMAR1
TFAP4
GNB2
LRP1
MDM2
DUSP1
POLR2H
CCND1
CCNE1
KRT18
RIN1
SACS
SACS3D1
ATM
E2F1
RAD23B
RB1CC1
ACTA2
GNAI1
MAP3K12
GADD45A
TP53
GPX1
CDK4
PCNA
C
Hp stomach colonization cfu/g tssue (x10^5)
1000
100
10
1
0.1
Usf1 +/+
Usf1 −/−
9 Months
12 Months
D
GADD45
CSB
HR23A
CDKN1A
PCNA
RAB31
Wild-type
Wild-type H. pylori
USF1-KO
USF1-KO H. pylori
Relative expression /TBP
Relative expression/TBP

Figure S3

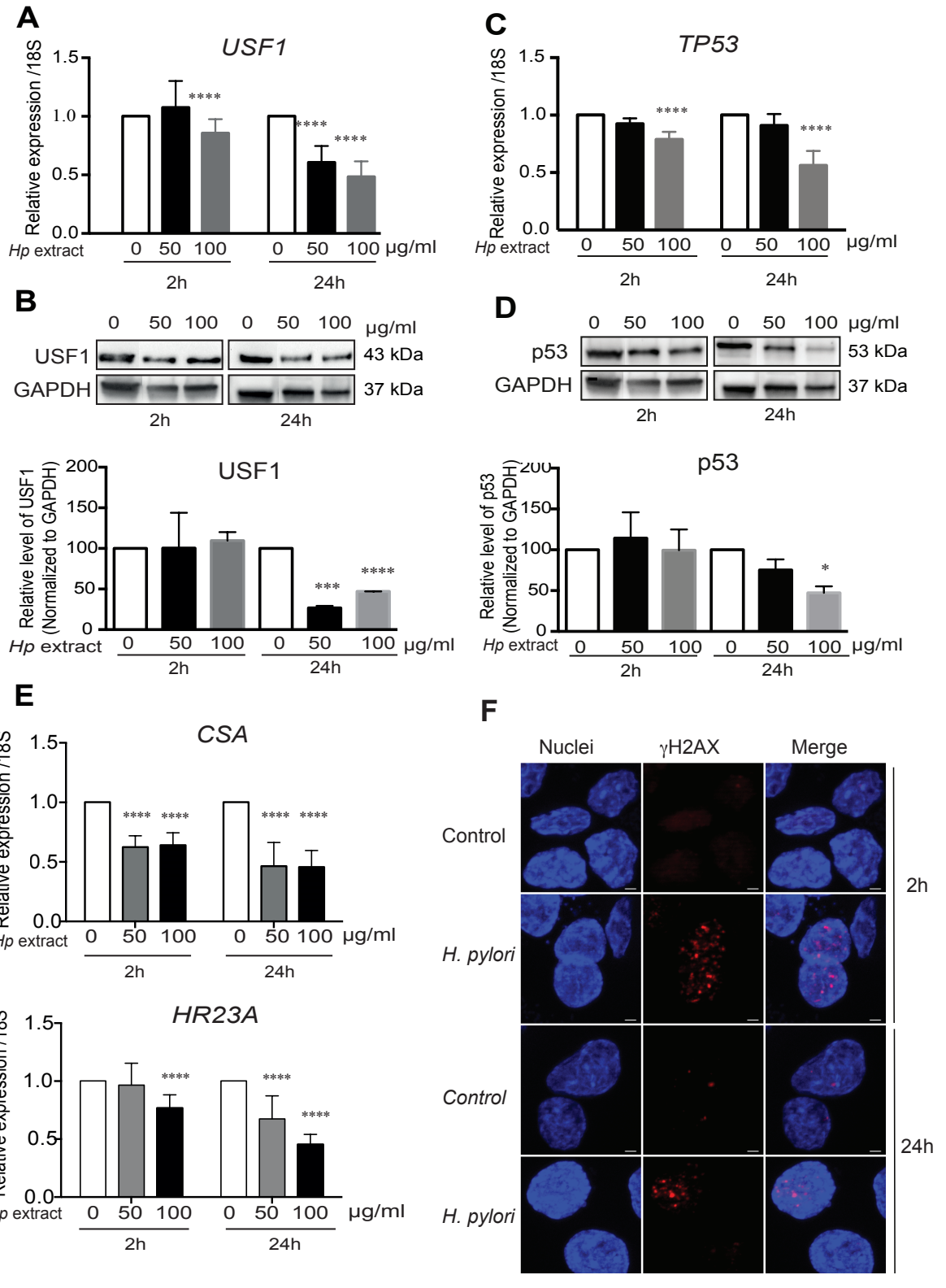
A
USF1
Relative expression /18S
1.5
1.0
0.5
0.0
****
****
****
Hp extract
0 50 100 0 50 100 µg/ml
2h
24h
C
TP53
Relative expression /18S
1.5
1.0
0.5
0.0
****
****
Hp extract
0 50 100 0 50 100 µg/ml
2h
24h
B
0 50 100 0 50 100 µg/ml
USF1
43 kDa
GAPDH
37 kDa
2h
24h
D
0 50 100 0 50 100 µg/ml
p53
53 kDa
GAPDH
37 kDa
2h
24h
USF1
Relative level of USF1 (Normalized to GAPDH)
200
150
100
50
0
***
****
Hp extract
0 50 100 0 50 100 µg/ml
2h
24h
p53
Relative level of p53 (Normalized to GAPDH)
200
150
100
50
0
*
Hp extract
0 50 100 0 50 100 µg/ml
2h
24h
E
CSA
Relative expression /18S
1.5
1.0
0.5
0.0
****
****
****
****
Hp extract
0 50 100 0 50 100 µg/ml
2h
24h
HR23A
Relative expression /18S
1.5
1.0
0.5
0.0
****
****
Hp extract
0 50 100 0 50 100 µg/ml
2h
24h
F
Nuclei
γH2AX
Merge
Control
H. pylori
Control
H. pylori
2h
24h

Figure S4

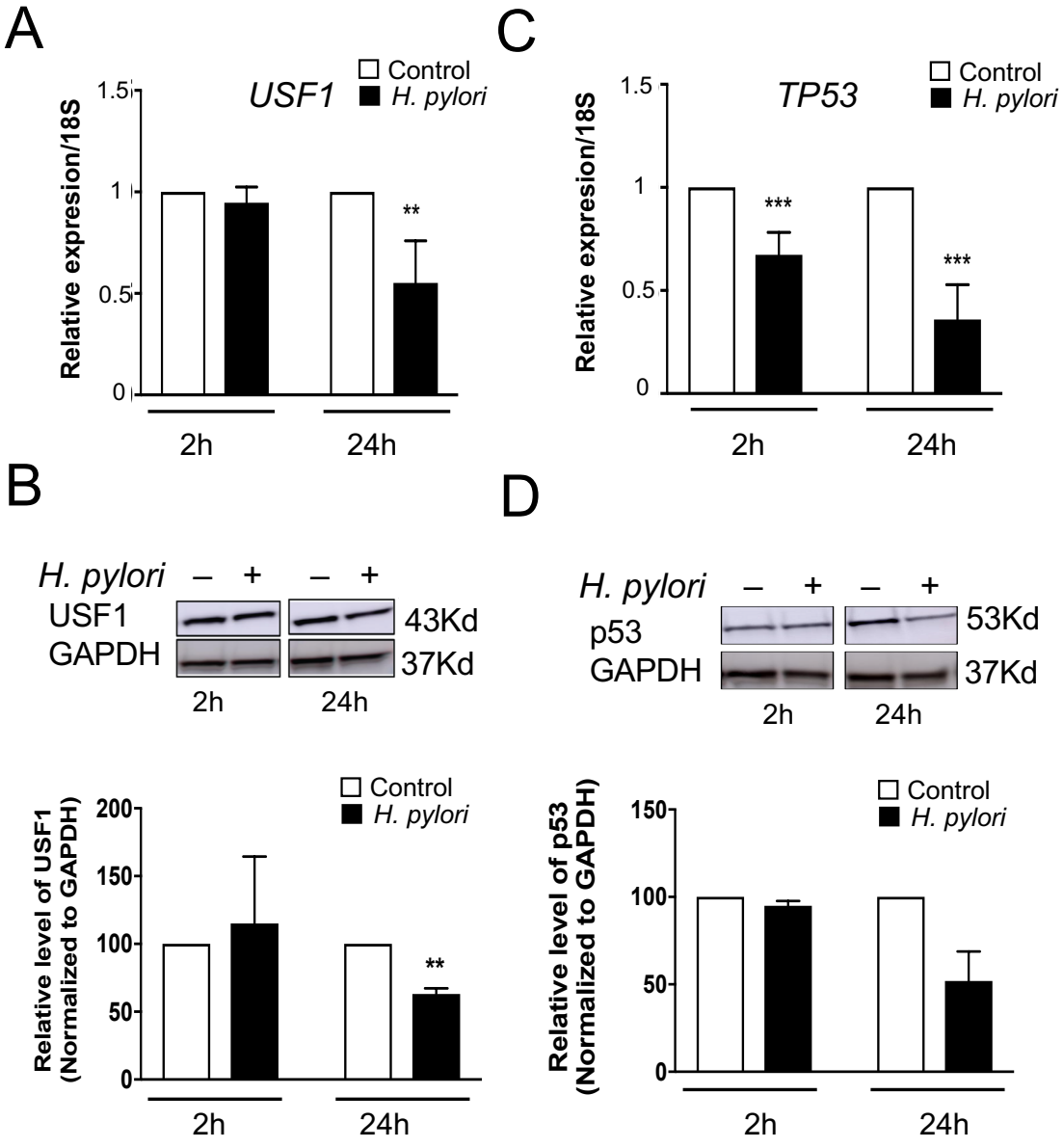
A
USF1
Control
H. pylori
Relative expresion/18S
1.5
1
0.5
0
**
2h
24h
C
TP53
Control
H. pylori
Relative expresion/18S
1.5
1
0.5
0
***
***
2h
24h
B
H. pylori – + – +
USF1
GAPDH
43Kd
37Kd
2h
24h
Control
H. pylori
Relative level of USF1 (Normalized to GAPDH)
200
150
100
50
0
**
2h
24h
D
H. pylori – + – +
p53
GAPDH
53Kd
37Kd
2h
24h
Control
H. pylori
Relative level of p53 (Normalized to GAPDH)
150
100
50
0
2h
24h

Figure S5

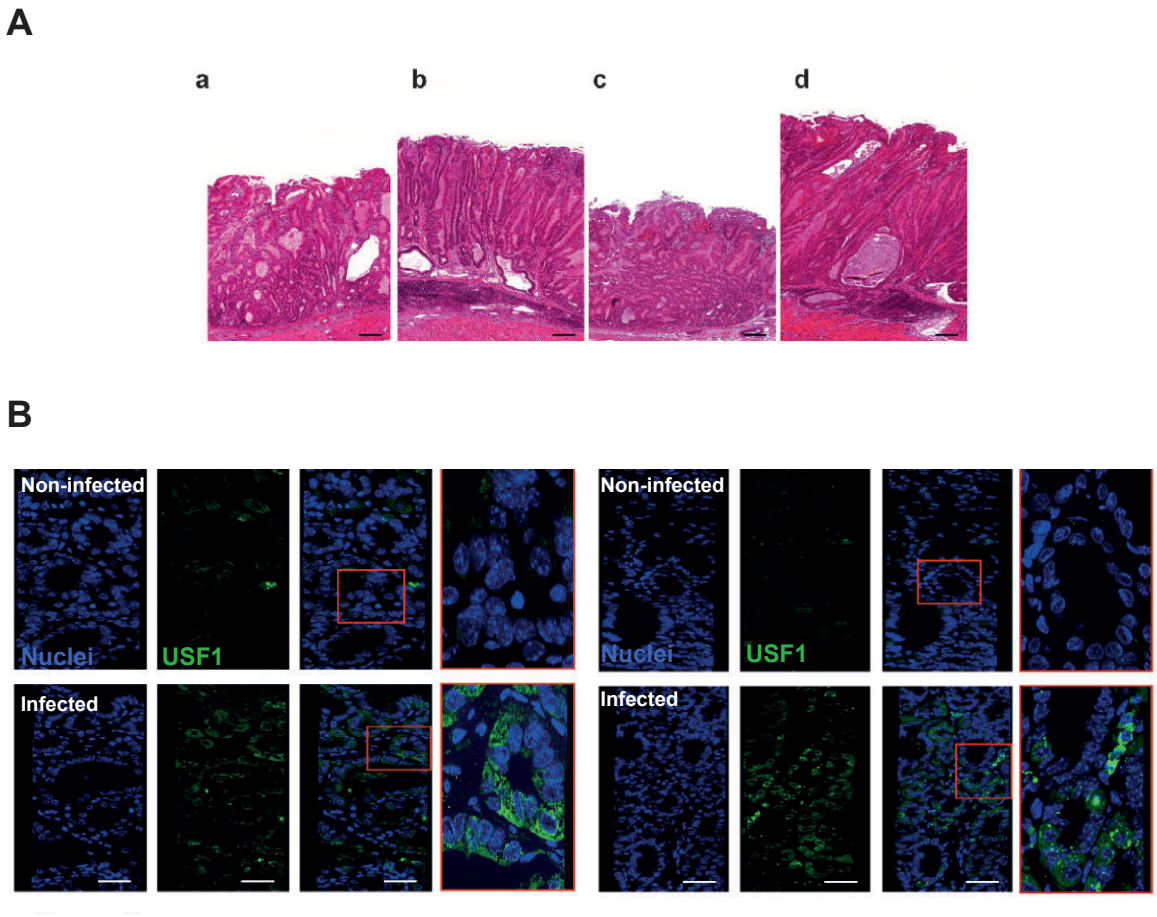
A
a
b
c
d
B
Non-infected
Nuclei
USF1
Infected
Non-infected
Nuclei
USF1
Infected
C
Non-infected
Nuclei
p53
Infected

Figure S6

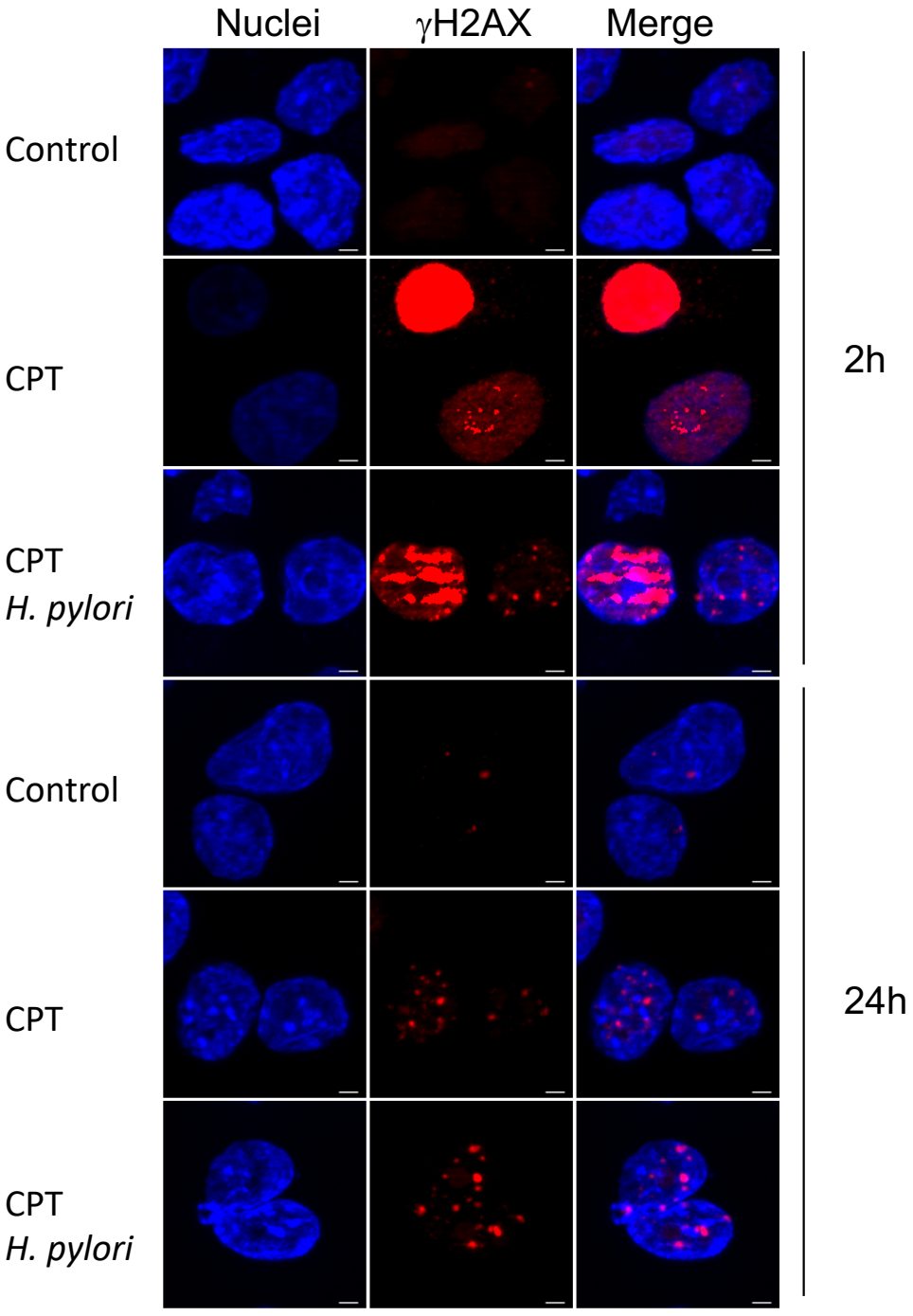
Nuclei
γH2AX
Merge
Control
CPT
CPT
H. pylori
2h
Control
CPT
CPT
H. pylori
24h

Figure S7

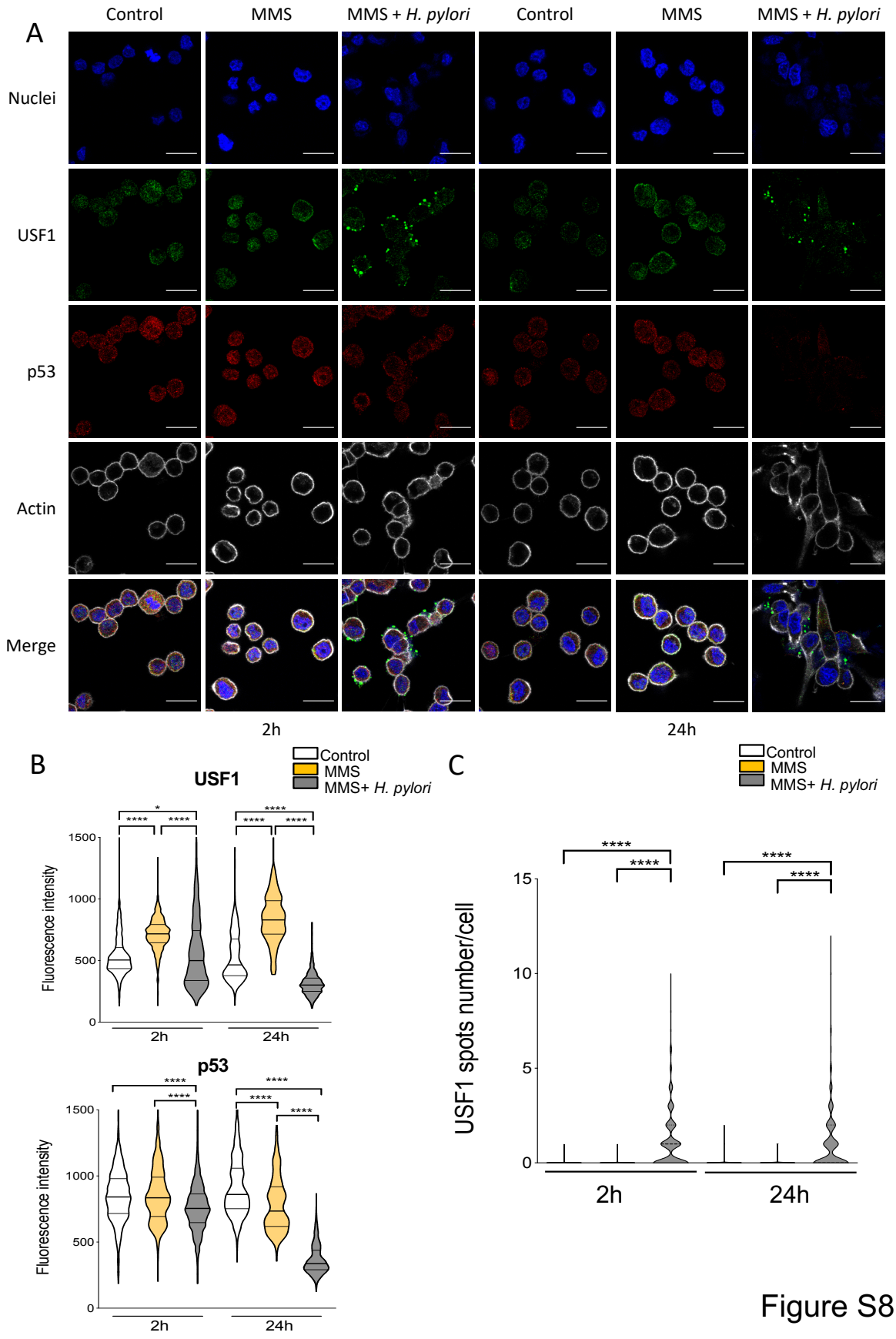
A
Control
MMS
MMS + H. pylori
Control
MMS
MMS + H. pylori
Nuclei
USF1
p53
Actin
Merge
2h
24h
B
USF1
Control
MMS
MMS+ H. pylori
Fluorescence intensity
1500
1000
500
0
2h
24h
p53
C
USF1 spots number/cell
15
10
5
0
****

Figure S8

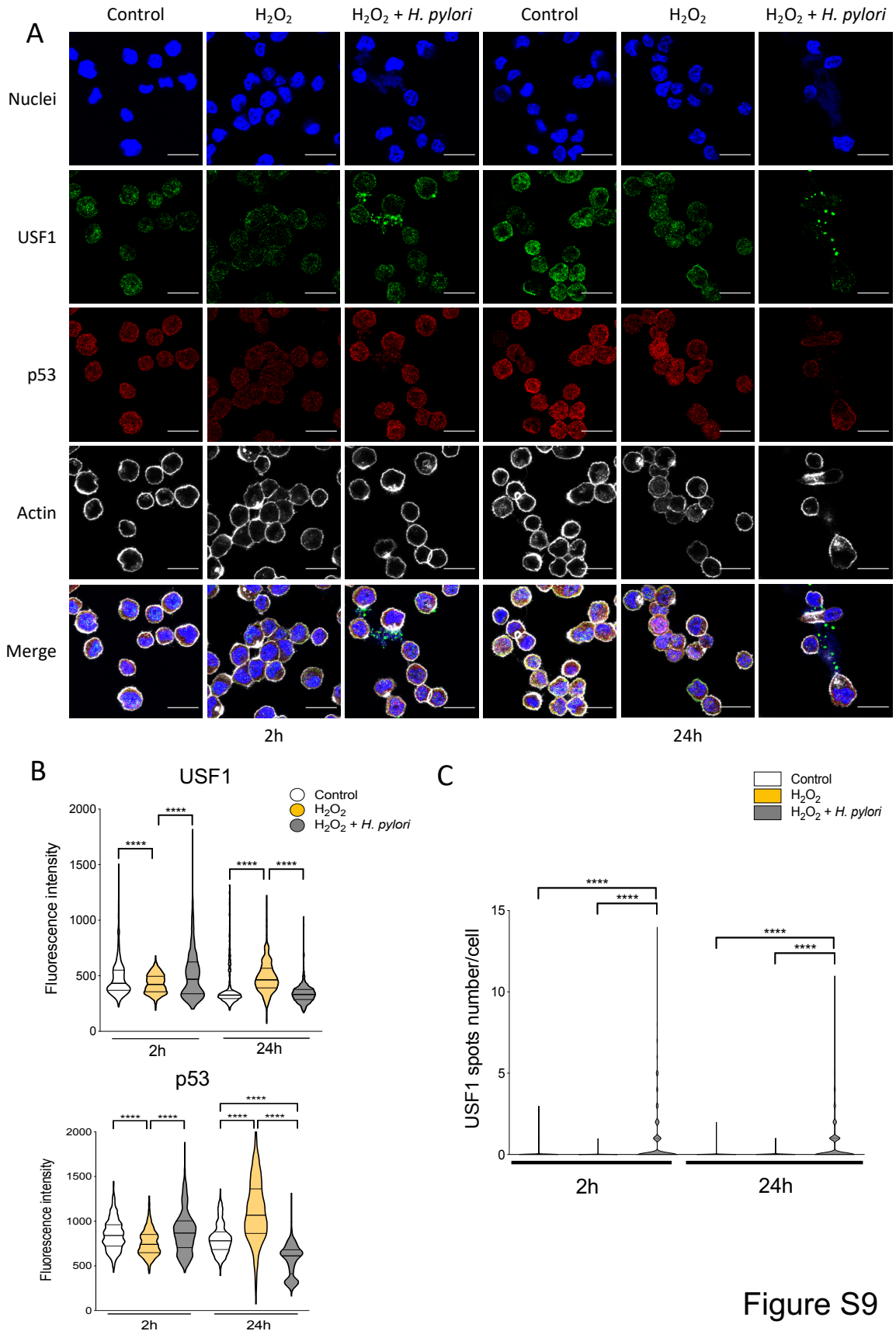
A
Control
H2O2
H2O2 + H. pylori
Control
H2O2
H2O2 + H. pylori
Nuclei
USF1
p53
Actin
Merge
2h
24h
B
USF1
Control
H2O2
H2O2 + H. pylori
Fluorescence intensity
2000
1500
1000
500
0
****
2h
24h
p53
C
USF1 spots number/cell
15
10
5
0

Figure S9

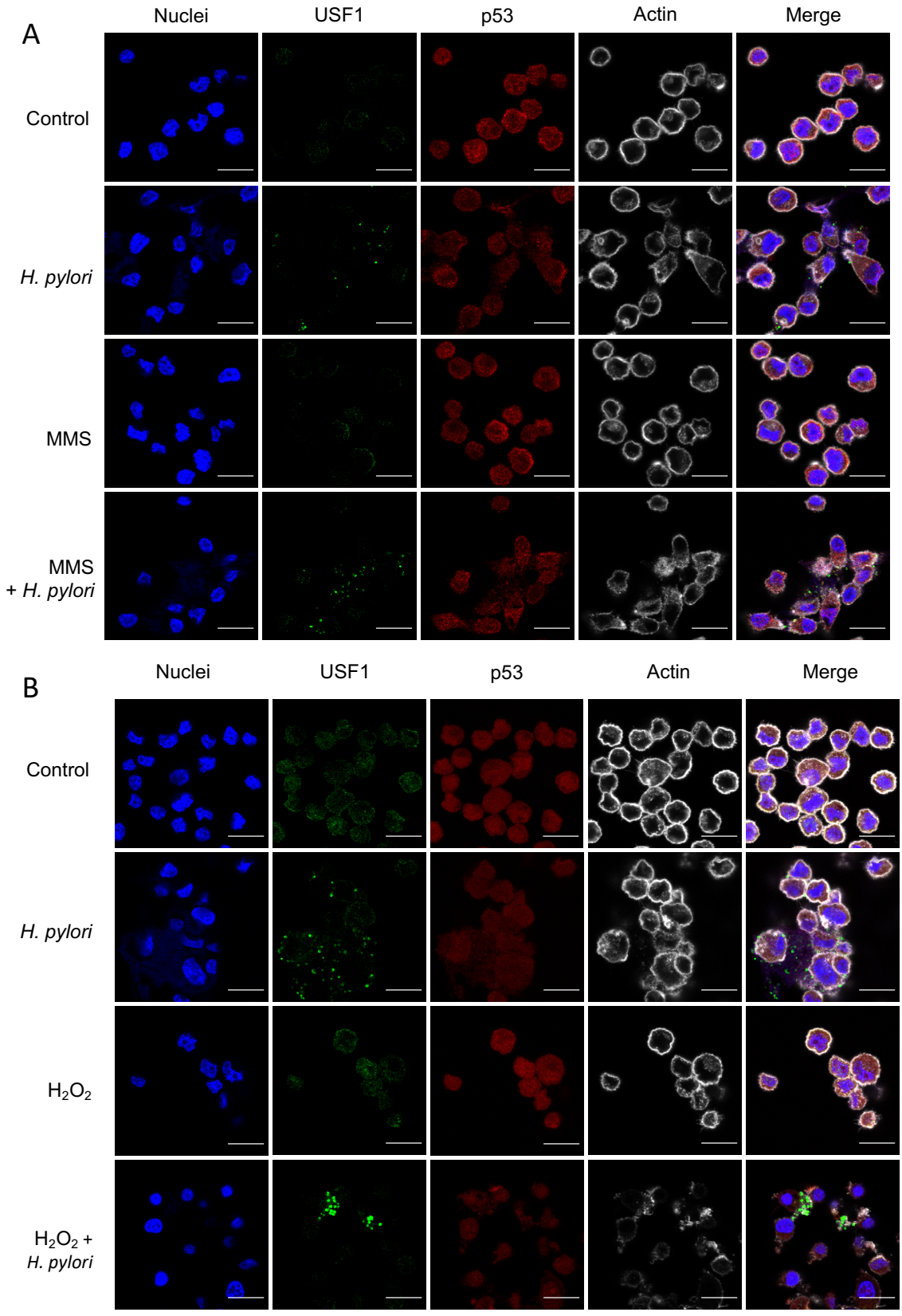
A
Nuclei
USF1
p53
Actin
Merge
Control
H. pylori
MMS
MMS
+ H. pylori
B
Nuclei
USF1
p53
Actin
Merge
Control
H. pylori
H2O2
H2O2 +
H. pylori

Figure S10